Chapter 3

Isolation and Characterization of Radical Anions Derived from a Boryl-Substituted Diphosphene

3-1, Introduction

Structural characterization of phosphorus-centered radicals has already described in chapter 1. Some diphosphenes can be reduced chemically or electro-chemically to afford the corresponding anion radicals (Scheme 1).[1] Such radical anions can also be generated by one-electron oxidation of dianionic diphosphanes or by fragmentation of dianionic tetraphosphanes.[2] Although these diphosphene radical anions could be detected by ESR spectroscopy, [hyperfine coupling constants: α(31P) = 41-55 G]. However, examples of stable diphosphene radical anions, which have been structurally characterized by X-ray diffraction analysis, have not been reported. Recently, isolation of carbene-coordinated P2 radical cation was reported, and this report showed that strongly electron donating carbene could stabilize radical cation of P2 species (Chapter 1.11).[3]

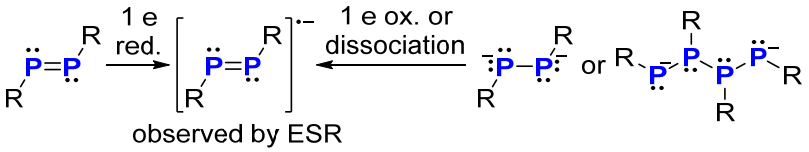

R = Mes*, $(Me_3Si)_3C$, 2,6-$Mes_2C_6H_3$, Tbt, Bbt, *t*-Bu, Ph, Cy
Mes* = 2,4,6-$^tBu_3C_6H_2$, Tbt = 2,4,6-$[(Me_3Si)_2CH]_3C_6H_2$
Bbt = 2,6-$[(Me_3Si)_2CH]_2$-4-$[(Me_3Si)_3C]C_6H_2$

Scheme 1. Methods to generate persistent diphosphene radical anions

Meanwhile, boryl-substituents exhibit extraordinary π-acceptor properties due to the vacant p-orbital on B that is able to accept electrons of adjacent heteroatoms with a lone pair. In borylphosphanes, the bond length of the B-P bond is generally shorter than those of phosphine-boranes on account of pπ-pπ interactions.[4] In addition, stabilization of anionic species by delocalization of electrons density to a vacant p orbital on B has also been reported. For example, the author has shown that π-acceptor properties of the boryl group were able to stabilize an anionic ^{n}BuLi adduct of diphosphene (Chapter 2).[5] Thus, the author expected that boryl group would stabilized radical anion of diphosphene through a delocalization of electrons to the boryl groups. In this chapter, the author will describe the synthesis and isolation of radical anions derived from diboryldiphosphene **113**, which were characterized experimentally by single-crystal X-ray diffraction analysis, ESR and UV-vis spectroscopy, as well as theoretically by DFT calculations. The latter showed in combination with the ESR results that spin density is delocalized over the B and P atoms on account of the π–accepting effect of the boryl groups.

3.2, Results and discussions

3.2.1, Synthesis of diboryldiphosphene radical anion

Cyclic voltammogram of boryl-substituted diphosphene **113** exhibited a reversible reduction wave at $E_{1/2}$ = -2.24 eV. The chemical one electron reduction of **113** with KC_8 in the presence/ absence of [2.2.2]-cryptand in THF at -35 ºC generated purple crystalline solids of radical anions [**113**$^{\cdot}$]$^-$[K(THF)$_2$]$^+$ and [**113**$^{\cdot}$]$^-$[K(cryptand)]$^+$ in 60% and 69% yield, respectively (Scheme 2), and these products were structurally characterized by single-crystal X-ray diffraction analysis (Figure 1). In the crystal, one of the two P atoms in [**113**$^{\cdot}$]$^-$[K(THF)$_2$]$^+$ is coordinated to a potassium cation to form a contact ion pair. The P-P bond lengths in [**113**$^{\cdot}$]$^-$[K(THF)$_2$]$^+$

[2.1112(9) Å] and [**113**$^{\cdot}$]$^{-}$[K(cryptand)]$^{+}$ [2.1453(19) Å] are longer than that in neutral diphosphene **113** [2.0655(17) Å] and those in the previously reported carbon-substituted diphosphenes [1.985(3)[6] – 2.051(2)[7] Å], but still shorter than conventional P-P single bonds (~ 2.2 Å).[8] In addition, the B-P bond distances in [**113**$^{\cdot}$]$^{-}$[K(THF)$_2$]$^{+}$ (av. 1.904 Å) and [**113**$^{\cdot}$]$^{-}$[K(cryptand)]$^{+}$ (av. 1.922 Å) contract upon the one-electron reduction of **113** [B-P: 1.936(3) Å]. The two B-containing planes in [**113**$^{\cdot}$]$^{-}$[K(THF)$_2$]$^{+}$ adopt an almost coplanar orientation with respect to the planar [B-P=P-B] moiety [P1-P2-B2-N3 175.22(15) and N1-B1-P1-P2 167.02(17)], while one of the two B-containing planes in [**113**$^{\cdot}$]$^{-}$[K(cryptand)]$^{+}$ is twisted relative to the P=P double bond [P1-P2-B2-N3 133.28(3), N1-B1-P1-P2 163.07(3)]. The structural features of these radical anions stand thus in stark contrast to the structure of **113**, in which both the two boron-containing planes adopt a perpendicular orientation relative to the central P=P double bond. The thus obtained structural data indicate that these radical anions exhibit a multiple-bond character for the P-P and P-B bonds, probably due to a delocalization of the unpaired electron and anionic charges over the [B-P-P-B] moiety.

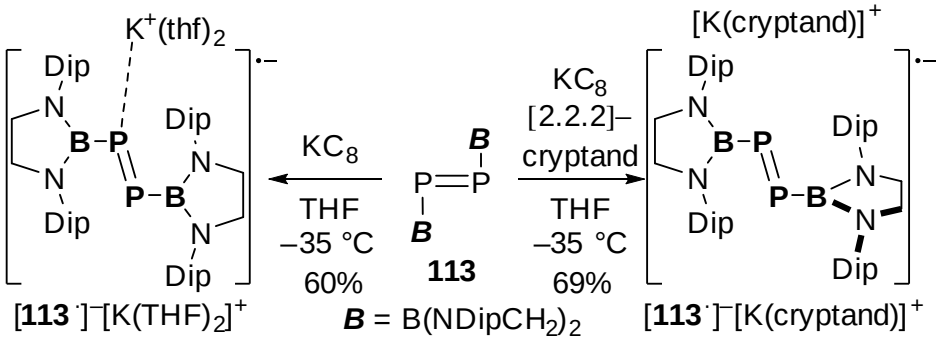

Scheme 2. Synthesis of the radical anions [**113**$^{\cdot}$]$^{-}$[K(THF)$_2$]$^{+}$ and [**113**$^{\cdot}$]$^{-}$[K(cryptand)]$^{+}$

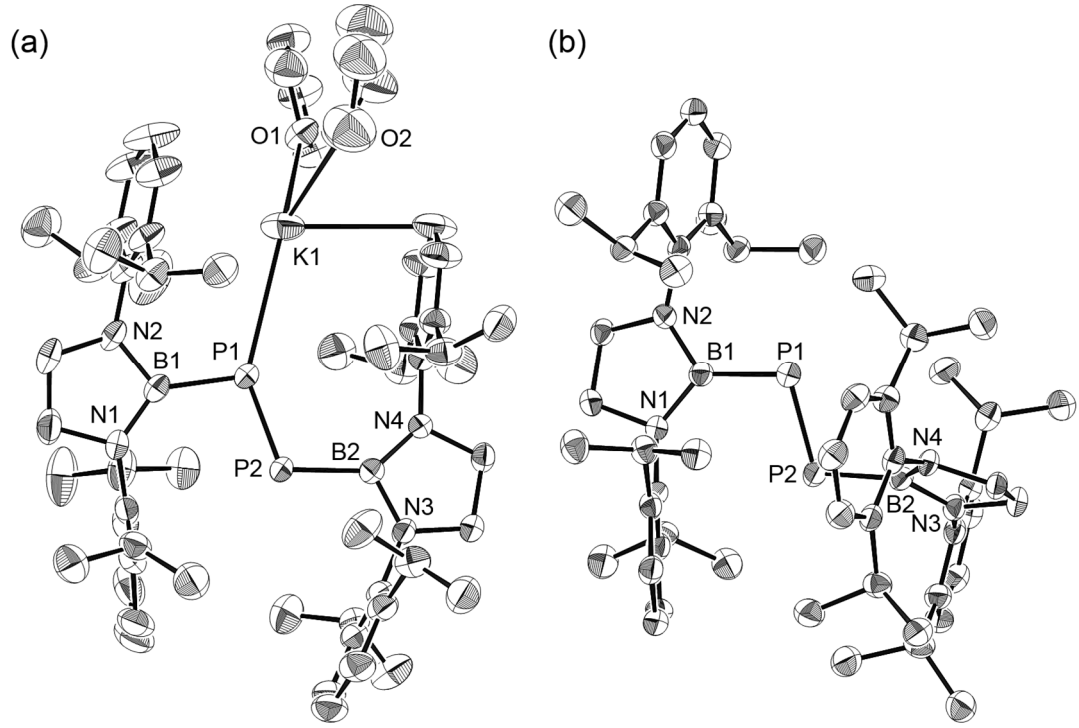

Figure 1. Crystal structures of [**113**$^{\cdot}$]$^{-}$[K(THF)$_2$]$^{+}$ and [**113**$^{\cdot}$]$^{-}$[K(cryptand)]$^{+}$ (thermal ellipsoids set at 50 % probability; hydrogen atoms, minor parts of disordered THF molecules, and [K(cryptand)]$^{+}$ cation are omitted for clarity). Selected bond lengths [Å] and angles [°] for [**113**$^{\cdot}$]$^{-}$[K(THF)$_2$]$^{+}$: P1-B1 1.901(3), P2-B2 1.907(3) B1-N1 1.444(3), B1-N2 1.444(3), B2-N3 1.430(3), B2-N4 1.432(3), P1-P2 2.1112(9), P1-P2-B2-N3 175.22(15), N2-B1-P1-P2 167.02(17); selected bond lengths [Å] and angles [°] for [**113**$^{\cdot}$]$^{-}$[K(cryptand)]$^{+}$: P1-B1 1.923(5), P2-B2 1.921(4) B1-N1 1.450(5), B1-N2 1.475(5), B2-N3 1.445(5), B2-N4 1.462(5), P1-P2 2.1452(19), P1-P2-B2-N3 133.28(3), N1-B1-P1-P2 163.07(3).

3.2.2, ESR and UV-vis absorption spectra of diboryldiphosphene radical anions

Both compounds exhibited identical ESR spectra at room temperature, which show that [**113**$^{\cdot}$]$^{-}$[K(THF)$_2$]$^{+}$ exists mainly as a separated ion pair in THF. In the ESR spectrum of [**113**$^{\cdot}$]$^{-}$ [K(cryptand)]$^{+}$, a triplet signal was observed at g = 2.013, which arises from the two magnetically equivalent P nuclei. (Figure 3) This result is comparable to those of previously reported diphosphene-derived radical anions (g = 2.007 – 2.018) (Table 1).[1] The magnitude of hyperfine coupling with the two phosphorus nuclei [α(^{31}P) = 37.3 G] is significantly smaller in [**113**$^{\cdot}$]$^{-}$[K(cryptand)]$^{+}$ than in all other previously reported persistent diphosphene radical anions (41-55 G). Including the contribution of the B nuclei [α(^{10}B) = 0.7 G; α(^{11}B) = 2.0 G] into a simulation allowed a close reproduction of the observed spectrum. These results indicate that, in contrast to the case of carbon-substituted diphosphenes, the electrons on the P atoms soaks into the vacant p-orbitals of the B atoms.

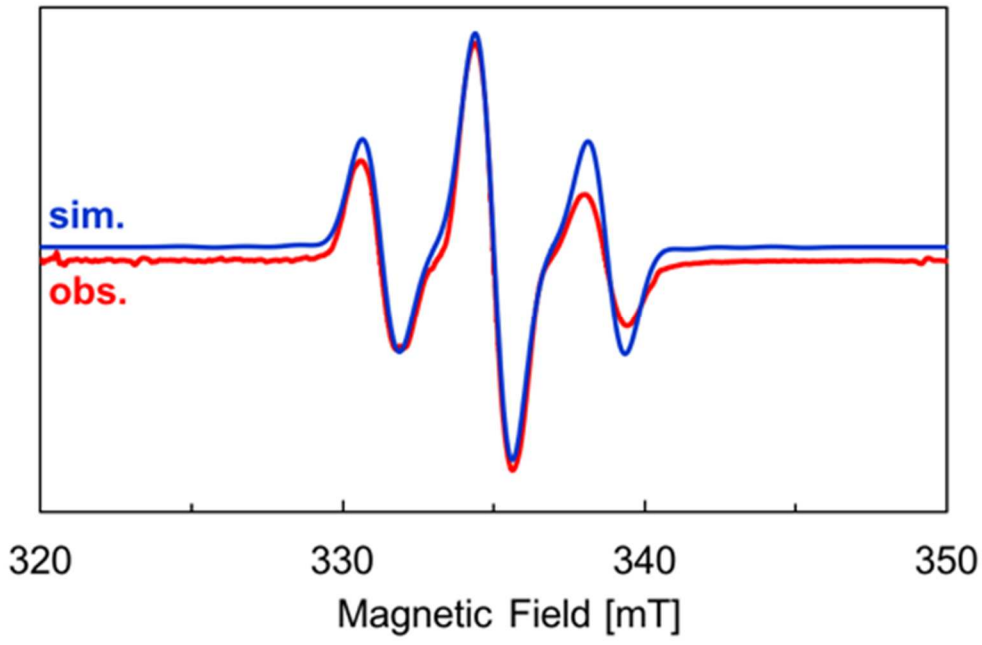

Figure 3. ESR spectrum of [**113**$^{\cdot}$]$^{-}$[K(cryptand)]$^{+}$ in THF at 298 K (red) and simulated ESR spectrum (blue) using the following parameters: g = 2.0125, α(^{31}P) = 37.3 G, α(^{10}B) = 0.7 G, and α(^{11}B) = 2.0 G. The simulation was performed on four isotopomers (^{11}B-^{11}B):(^{11}B-^{10}B):(^{10}B-^{11}B):(^{10}B-^{10}B) in a 64:16:16:4 ratio (calculated from the natural abundance of boron nuclei; ^{11}B/^{10}B=80:20).

The difference between observed and simulated spectra at ~337 mT is due to a slow tumbling motion on the ESR timescale. The UV-vis absorption spectra of these radical anions in THF showed characteristic absorption maxima at 513 nm (Figure 4), which are slightly blue-shifted compared to those of previously reported diphosphene radical anions. The identical absorption maxima and ESR spectra of these two species supported the notion that [**113**$^{\cdot}$]$^{-}$[K(THF)$_2$]$^{+}$ exists as a separated ion pair in THF. In the longer wavelength region, shoulders of relatively low intensity were observed at ~670 nm (ε 80-140), which are red-shifted in comparison to that of a Tbt-substituted diphosphene radical anion.[1] This shift should be attributed to the energetic lowering of the SOMO on account of the π-accepting substituent effect of the boryl groups. As a result, the absorption edge extends up to 750 nm. Based on time-dependent DFT (TD-DFT) calculations on [**113**$^{\cdot}$]$^{-}$, these absorptions were assigned to SOMO-related transitions, including a symmetry forbidden *n*-SOMO transition with a small oscillator strength (*f* = 0.0001) at 726 nm (for details of the DFT calculations, *vide infra*).

Table 1. ESR data of a variety diphosphene anion radical at room temperature.

	g value	*a*(^{31}P) (G)
$Tbt_2P_2^{\cdot-}$ [a]	2.010	47.6
$Bbt_2P_2^{\cdot-}$ [a]	2.009	48.0
$Mes^*P_2^{\cdot-}$	2.010[b]/2.013[c]	55[b]/55[c]
$Tsi_2P_2^{\cdot-}$	2.018[c]/2.0111[d]	43[c]/43.5[d]
$Ar_2P_2^{\cdot-}$	2.007	46
$^tBu_2P_2^{\cdot-}$ [f]	2.0103	45.47
$Ph_2P_2^{\cdot-}$ [g]	2.0089	40.9
$Cy_2P_2^{\cdot-}$ [g]	2.0099	45.2

[a] In THF solution of isolated $[Li(dme)_3]^+[Ar_2P_2]^{\bullet-}$ (Ar = Tbt or Bbt).
[b] Generated by the reduction of neutral $Mes_2{}^*P_2$ with sodium naphthalenide in THF.
[c] Generated by the bulk electrolysis in THF (*n*-Bu_4NBF_4).
[d] Generated by the bulk electrolysis in DME (0.1 M *n*-Bu_4NBF_4).
[e] Generated by the reduction of neutral (Ar = 2,6-dimesityl-*p*-tolyl) with sodium metal or potassium napthalenide in THF.
[f] Generated from $K_2[^tBu_2P_2]$ in THF.
[g] Generated from $Na_2[R_4P_4]$ in THF (R = phenyl or cyclohexyl).

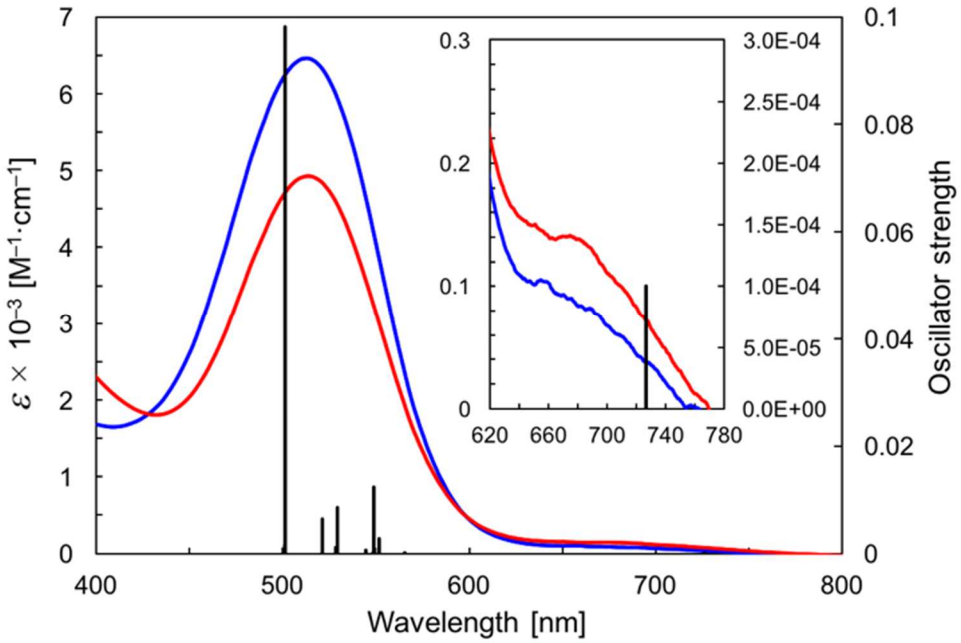

Figure 4. UV-vis spectra of [**113**$^{\cdot}$]$^{-}$[K(THF)$_2$]$^{+}$ (red) and [**113**$^{\cdot}$]$^{-}$[K(cryptand)]$^{+}$ (blue) in THF (125 μM) at room temperature, together with transitions of [**113**$^{\cdot}$]$^{-}$ (black) calculated at the UB3LYP/6-31G(d) level of theory; inset: expanded spectra and oscillator strength for the 620-780 nm region.

3.2.3, Stability of diboryldiphosphene radical anions in THF

The thermal stability of [**113**$^{\cdot}$]$^{-}$[K(THF)$_2$]$^{+}$ was estimated by UV-vis spectroscopy. Leaving a THF solution of [**113**$^{\cdot}$]$^{-}$[K(THF)$_2$]$^{+}$ led to decreasing of the absorption at 513 nm (Figure 4). After 6 h, the absorbance of [**113**$^{\cdot}$]$^{-}$[K(THF)$_2$]$^{+}$ decreased to about half of the original value. While, the decomposition of [**113**$^{\cdot}$]$^{-}$[K(cryptand)]$^{+}$ was slower than that of [**113**$^{\cdot}$]$^{-}$[K(THF)$_2$]$^{+}$ (Figure 5). Thus, the separation of K^{+} from diphosphene radical anion improved its thermal stability.

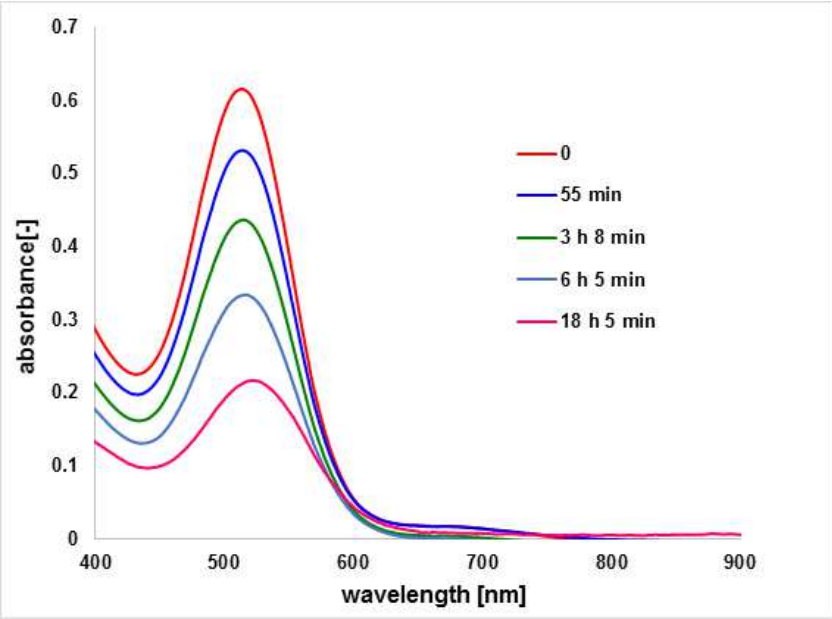

Figure 4. UV-vis spectra of [**113**$^{\cdot}$]$^{-}$[K(THF)$_2$]$^{+}$ in THF at room temperature (the reaction time; 0, 55 min, 3 h 8 min, 6 h 5 min, 18 h 5 min)

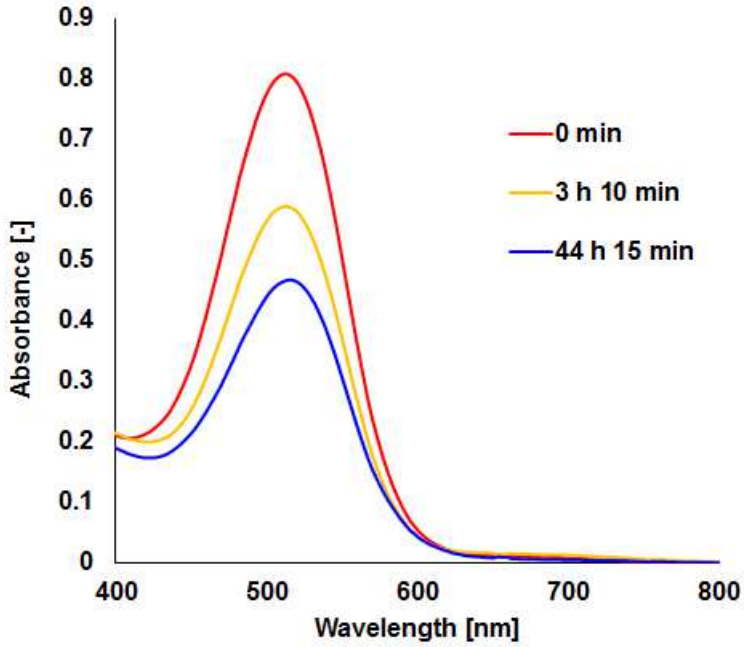

Figure 5. UV-vis spectra of [**113**$^{\cdot}$]$^{-}$[K(cryptand)]$^{+}$ in THF at room temperature (the reaction time; 0, 3 h 10 min, 44 h 15 min)

3.2.4, DFT calculations of diboryldiphosphene radical anion

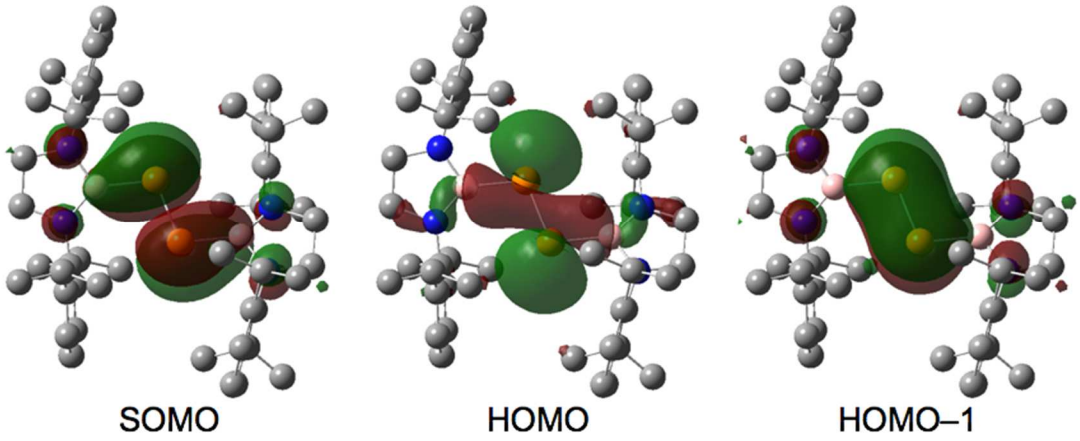

Figure 7. Selected molecular orbitals of free radical anion [**113**$^{\cdot}$]$^{-}$ calculated at the UB3LYP/6-31G(d) level of theory (hydrogen atoms omitted for clarity, gray: carbon, blue: nitrogen, orange: phosphorus, pale peach: boron)

DFT calculations on the free radical anion [**113**$^{\cdot}$]$^{-}$ revealed characteristic molecular orbitals that describe pπ-pπ interactions between the B and P atoms (Figure 7). Using the anionic part of [**113**$^{\cdot}$]$^{-}$[K(THF)$_2$]$^{+}$ in the crystal structure as an initial geometry, the optimized structure of [**113**$^{\cdot}$]$^{-}$ revealed two B-containing planes that adopted an almost coplanar orientation relative to the [B-P=P-B] moiety, which stands in contrast to the experimentally obtained structure of [**113**$^{\cdot}$]$^{-}$[K(THF)$_2$]$^{+}$.[9] The SOMO of [**113**$^{\cdot}$]$^{-}$ consists of a π*-type orbital of the P=P moiety in **113** and two vacant p-orbitals on the B atoms, indicating a delocalization of spin density over the [B-P=P-B] moiety. The HOMO and HOMO-1 correspond to lone pairs on the P atoms and a bonding π-orbital, respectively. These results are consistent with an elongation of the P-P bond and a contraction of the B-P bonds in [**113**$^{\cdot}$]$^{-}$[K(THF)$_2$]$^{+}$ and [**113**$^{\cdot}$]$^{-}$[K(cryptand)]$^{+}$. The Wiberg bond indexes of [**113**$^{\cdot}$]$^{-}$ (P-B: 1.21, 1.21; P-P: 1.26) also support a multiple-bond character, which is consistent with the delocalization of the unpaired electron density over the [B-P=P-B] moiety (Table 2). The calculated Mulliken spin density distribution (P: 0.415, 0.407; B 0.042, 0.043) agreed well with the hyperfine coupling constants observed in the ESR spectrum. The results of an NBO analysis on [**113**$^{\cdot}$]$^{-}$ suggest that donor-acceptor interactions exist between P and B (second-order perturbation energies: 29.63 and 29.58 kcal/mol), and that they are comparable to those between N and B (~26 kcal/mol).

Table 2. Selected Mulliken spin densities, Wiberg bond indexes (WBI), donor-acceptor interaction (kcal/mol) in free [**113**$^{\cdot}$]$^{-}$ from [**113**$^{\cdot}$]$^{-}$[K(THF)$_2$]$^{+}$

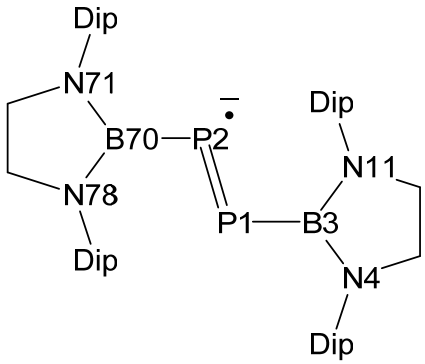

atom	spin density	bond	WBI	donor	acceptor	interaction
P1	0.415059	P1-P2	1.2555	P1	B3	29.67
P2	0.406843	P1-B3	1.2088	P2	B70	29.58
B3	0.041604	P2-B70	1.2099	N4	B3	26.51
B70	0.043364	B3-N4	0.9023	N11	B3	25.38
N4	0.013864	B3-N11	0.8867	N71	B70	26.84
N11	0.022139	B70-N71	0.9024	N78	B70	25.58
N71	0.013381	B70-N78	0.8858	P1-P2	B3	9.48
N78	0.020631			P1-P2	B70	9.51

Considering these results in their entity, the radical anion [**113**$^{\cdot}$]$^{-}$ is characterized by a π-accepting effect of the boryl substituents and should be described ideally by resonance structures **A**-**D** (Scheme 2), which are consistent with an elongated P-P bond, contracted B-P bonds, and a distribution of the unpaired electron that is predominantly centered on the P atoms, but contains also small yet significant contributions from B atoms.

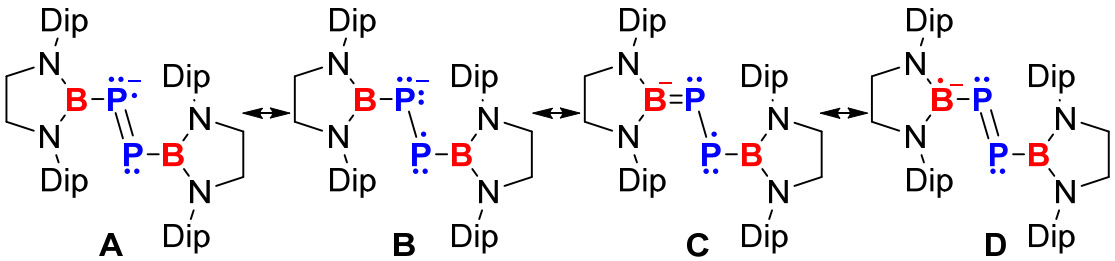

Scheme 2. Resonance structures **A**-**D** for radical anion [**113**$^{\cdot}$]$^{-}$ (for each structure an isomer exists that is obtained from a 180° rotation around the C_2 axis bisecting the P-P bond).

3.3, Conclusion

In summary, the diphosphene radical anions [**113**$^{\cdot}$]$^{-}$[K(THF)$_2$]$^{+}$ and [**113**$^{\cdot}$]$^{-}$[K(cryptand)]$^{+}$ were isolated and characterized by single-crystal X-ray diffraction analysis, UV-vis and ESR spectroscopy, as well as DFT

calculations. The results revealed that the radical anions are characterized by the π-accepting properties of the boryl substituents, and that the spin density is delocalized over the B-P=P-B moiety.

Experimental procedure

General procedures

All manipulations involving the air- and moisture-sensitive compounds were carried out in a glovebox (Korea KIYON) under argon. THF, toluene, and *n*-hexane were purified by passing through a solvent purification system (Grass Contour). THF was degassed and was dried by stirring with Na/K alloy at room temperature in the glovebox prior to use. Potassium (purchased from Kanto Chemical Co., Inc., containing 0.1% sodium and 0.001% silicon) was washed with hexane before the use. Melting points were determined on Optimelt (SRS) and were uncorrected. Elemental analyses were performed on a Perkin Elmer 2400 series II CHN analyzer. X-ray crystallographic analysis was performed on VariMax/Saturn CCD diffractometer. UV/vis spectrum was recorded on DT-MINI-2-GS (Ocean Optics). ESR spectra were recorded on JES-X330 (JEOL) and were fitted with simulated spectrum to calculate hyperfine coupling constants. KC_8 and boryl-substituted diphosphene **113** were synthesized according to the literature procedure. [5][10]

Synthesis of $[\mathbf{113}^{\cdot}]^{-}[K(THF)_2]^{+}$

In a glovebox, precooled THF (5 mL) at –30 ºC was added to a mixture of **113** (80.0 mg, 95.2 μmol) and KC_8 (15.4 mg, 114 μmol) in a 15 mL vial. The color of the resulting solution rapidly turned into violet. After the reaction mixture was stirred at –30 ºC for 2 h, the resulting suspension was filtered through a pad of Celite to remove graphite. Removal of solvents from the filtrate under reduced pressure formed a purple solid. The residue was recrystallized from hexane/THF to give $[\mathbf{113}^{\cdot}]^{-}[K(THF)_2]^{+}$ as purple crystals (58.4 mg, 57.0 μmol, 60 %). mp: 248.2-249.9 ºC (dec.). It was difficult to obtain satisfactory data of elemental analysis because of rapid decomposition.

Synthesis of $[\mathbf{113}^{\cdot}]^{-}[K(cryptand)]^{+}$

In a glovebox, precooled THF (4.4 mL) at –30 ºC was added to a mixture of **113** (70.0 mg, 83.2 μmol), KC_8 (13.5 mg, 100 μmol), and [2.2.2]-cryptand (37.6 mg, 100 μmol) in a 15 mL vial. The color of the resulting solution rapidly turned into violet. After the reaction mixture was stirred at –30 ºC for 2 h, the resulting suspension was filtered through a pad of Celite to remove graphite. Removal of solvents from the filtrate under reduced pressure formed a purple solid. The residue was recrystallized from toluene/THF to give $[\mathbf{113}^{\cdot}]^{-}[K(cryptand)]^{+}$ as purple crystals (72.3 mg, 57.5 μmol, 69 %). mp: 207.7-208.6 ºC (dec.). Anal. calcd. for $C_{70}H_{112}B_2KN_6O_6P_2$: C, 66.9; H, 8.99; N, 6.69. Found: C, 66.6; H, 9.38; N, 6.67.

ESR spectra of $[\mathbf{113}^{\cdot}]^{-}[K(THF)_2]^{+}$ and $[\mathbf{113}^{\cdot}]^{-}[K(cryptand)]^{+}$

A solid of each compound was dissolved in a quartz glass tube by vacuum distillation of THF under reduced pressure. Before melting the solvents, the resulting sample was sealed with flame under reduced pressure. The ESR spectrum of each sample was recorded at room temperature (Figure S1). The sample of $[\mathbf{113}^{\cdot}]^{-}[K(THF)_2]^{+}$

was further heated at 50 °C for 5 min and at 80 °C for 15 min, and then ESR spectrum was recorded with Mn marker (Figure S2).

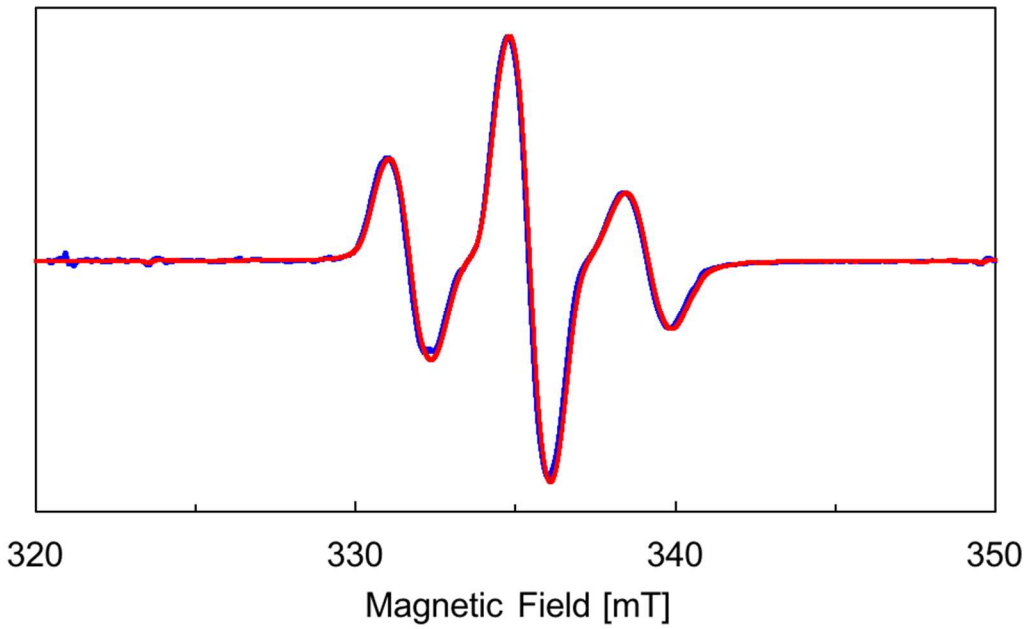

Figure S1. ESR spectra of [**113**$^{\cdot}$]$^{-}$[K(THF)$_2$]$^{+}$ (red) and [**113**$^{\cdot}$]$^{-}$[K(cryptand)]$^{+}$ (blue) with normalization of the intensity

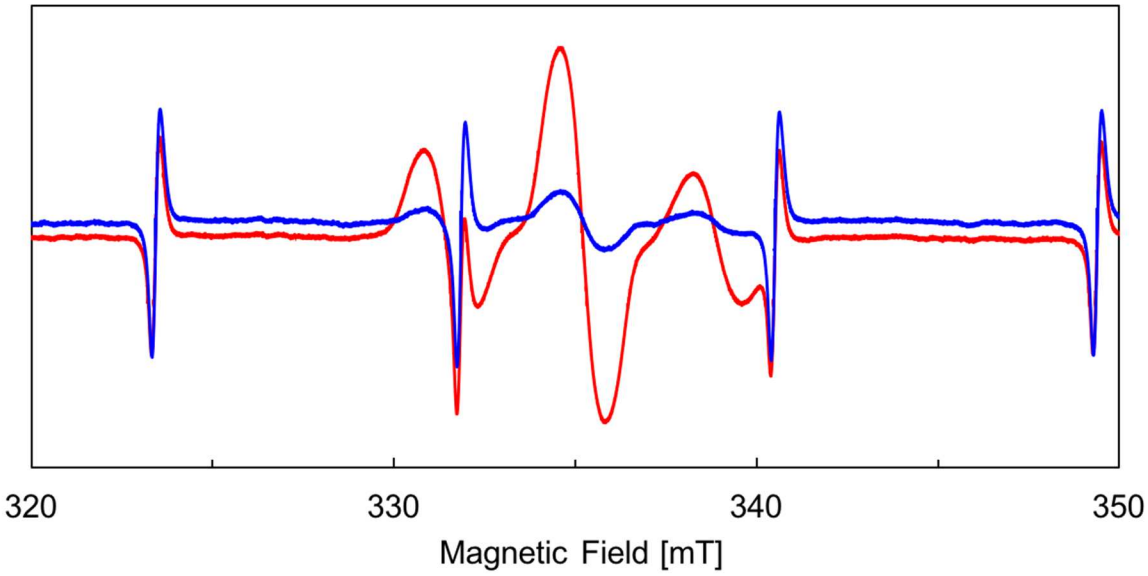

Figure S2. ESR spectrum of [**113**$^{\cdot}$]$^{-}$[K(THF)$_2$]$^{+}$ with Mn marker (red) and ESR spectrum of the same sample after heating at 80 °C (blue)

2. Details for X-Ray Crystallography

Details of the crystal data and a summary of the intensity data collection parameters [**113**$^{\cdot}$]$^{-}$[K(THF)$_2$]$^{+}$ and

[**113**$^{\cdot}$]$^{-}$[K(cryptand)]$^{+}$ are listed in Table S1.In each case a suitable crystal was mounted with a mineral oil to the glass fiber and transferred to the goniometer of a VariMax Saturn CCD diffractometer with graphite-monochromated Mo Kα radiation (λ = 0.71075 Å). All the following procedure for analysis, Yadokari-XG 2009 was used as a graphical interface.[11] The structures were solved by direct method with (SIR-2014 and SIR-97)[12] and refined by full-matrix least-squares techniques against F^2 (SHELXL-2014).[13] The intensities were corrected for Lorentz and polarization effects or NUMABS program (Rigaku 2005). The non-hydrogen atoms were refined anisotropically. Hydrogen atoms were placed using AFIX instructions.

Table S1. Crystallographic data and structure refinement details for [**113**$^{\cdot}$]$^{-}$[K(THF)$_2$]$^{+}$ and [**113**$^{\cdot}$]$^{-}$[K(cryptand)]$^{+}$

	[**113**$^{\cdot}$]$^{-}$[K(THF)$_2$]$^{+}$	[**113**$^{\cdot}$]$^{-}$[K(cryptand)]$^{+}$
Empirical formula	$C_{60}H_{92}B_2KN_4O_2P_2$	$C_{70}H_{112}B_2KN_6O_6P_2$
Formula weight	1024.03	1256.37
T (K)	143	93
λ (Å)	0.71069	0.71075
Crystal system	Monoclinic	Triclinic
Space group	$P2_1/n$	P-1
a (Å)	12.231(5)	12.501(11)
b (Å)	19.225(5)	17.072(13)
c (Å)	26.393(5)	18.253(15)
α (°)	90	90.396(15)
β (°)	96.723(5)	106.933(18)
γ (°)	90	91.928(14)
V (Å^3)	6163(3)	3724(5)
Z	4	2
$D_{calc,}$ (g/m^3)	1.104	1.120
μ (mm^{-1})	0.180	0.165
F(000)	2220	1362
Crystal size (mm)	0.21×0.12×0.07	0.14×0.14×0.13
2θ range (°)	3.018-27.485	3.003-27.226
reflns collected	50366	28946
Indep reflns/ R_{int}	14121/0.0482	15917/0.0590
param	747	800
GOF on F^2	1.041	1.060
R_1, wR_2 [I>2σ(I)]	0.0802, 0.2110	0.0869, 0.1887
R_1, wR_2 (all data)	0.1072, 0.2399	0.1416, 0.2307

3. Computational Detail

The geometry optimizations were performed at the B3LYP[14]/6-31G(d)[15] level of theory by using Gaussian 09 program package[16] for the contact ion pair of [**113**$^{\cdot}$]$^{-}$[K(THF)$_2$]$^{+}$ and for two types of free radical anion [**113**$^{\cdot}$]$^{-}$ from the crystal structures of [**113**$^{\cdot}$]$^{-}$[K(THF)$_2$]$^{+}$ and [**113**$^{\cdot}$]$^{-}$[K(cryptand)]$^{+}$. The optimized structure was confirmed to have no imaginary frequency and could reproduce the X-ray structure (Figure S3). For evaluation of molecular orbitals, single point calculations were also performed with UHF/6-31G(d) level of theory with optimized structures. At the optimized structures, natural bond orbital (NBO) analysis was performed at B3LYP[14]/6-31G(d)[15] level of theory for estimation of Wiberg bond index (WBI) and Mulliken atomic densities by using NBO 3.0 package embedded in Gaussian program.[17] The TD-DFT calculation was performed at the UB3LYP/6-31G(d) level of theory (Table S2 and Figure S4).

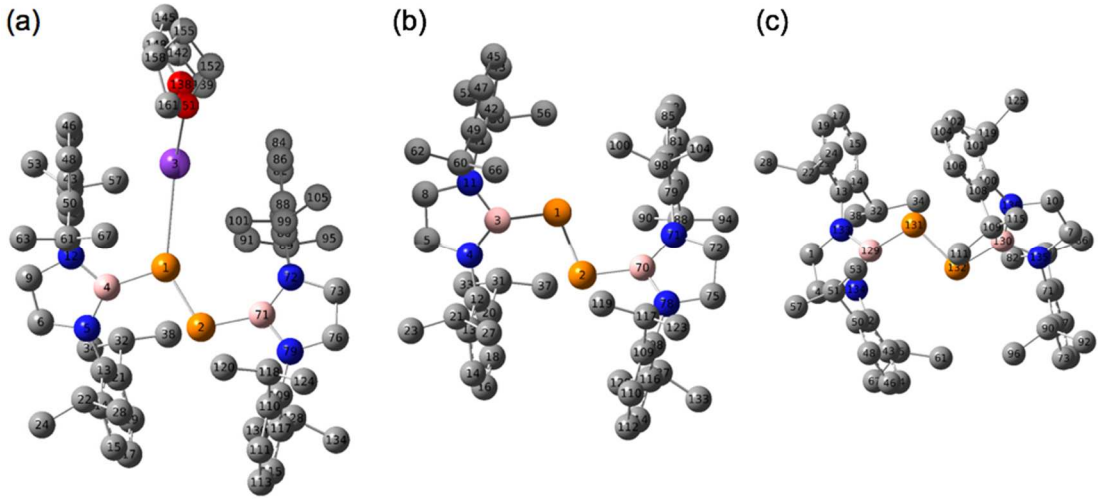

Figure S3. The optimized structures of (a) [**113**$^{\cdot}$]$^{-}$[K(THF)$_2$]$^{+}$, (b) free [**113**$^{\cdot}$]$^{-}$ from [**113**$^{\cdot}$]$^{-}$[K(THF)$_2$]$^{+}$, (c) free [**113**$^{\cdot}$]$^{-}$ from [**113**$^{\cdot}$]$^{-}$[K(cryptand)]$^{+}$.

Table S2. Calculated excitation energies of free [**113**$^{\cdot}$]$^{-}$ from [**113**$^{\cdot}$]$^{-}$[K(THF)$_2$]$^{+}$ by TD-DFT method (SOMO = 229)

Excited State 1:	2.002-A	1.7069 eV	726.36 nm	f=0.0001	<S**2>=0.752
228B -> 229B	0.99396				
Excited State 2:	2.009-A	2.1928 eV	565.42 nm	f=0.0001	<S**2>=0.759
229A -> 230A	0.94876				
229A -> 231A	0.11646				
229A -> 232A	0.23691				
229A -> 233A	-0.12855				
Excited State 3:	2.009-A	2.2473 eV	551.70 nm	f=0.0028	<S**2>=0.760
229A -> 230A	-0.13199				
229A -> 231A	0.69147				
229A -> 232A	0.46673				

229A -> 233A 0.52576

Excited State 4: 2.009-A 2.2601 eV 548.59 nm f=0.0124 <S**2>=0.759

229A -> 231A 0.70294

229A -> 232A -0.41111

229A -> 233A -0.56982

Excited State 5: 2.009-A 2.2759 eV 544.77 nm f=0.0005 <S**2>=0.759

229A -> 230A -0.25766

229A -> 232A 0.73760

229A -> 233A -0.60681

Excited State 6: 2.005-A 2.3420 eV 529.39 nm f=0.0085 <S**2>=0.755

229A -> 234A 0.40399

229A -> 235A 0.87457

227B -> 229B -0.25292

Excited State 7: 2.005-A 2.3463 eV 528.42 nm f=0.0010 <S**2>=0.755

229A -> 234A 0.90826

229A -> 235A -0.39889

Excited State 8: 2.006-A 2.3786 eV 521.25 nm f=0.0064 <S**2>=0.756

229A -> 236A 0.97593

227B -> 229B 0.17533

Excited State 9: 2.007-A 2.3918 eV 518.37 nm f=0.0002 <S**2>=0.757

229A -> 237A 0.98977

Excited State 10: 2.000-A 2.4741 eV 501.14 nm f=0.0981 <S**2>=0.750

229A -> 235A 0.27179

229A -> 236A -0.17341

227B -> 229B 0.92415

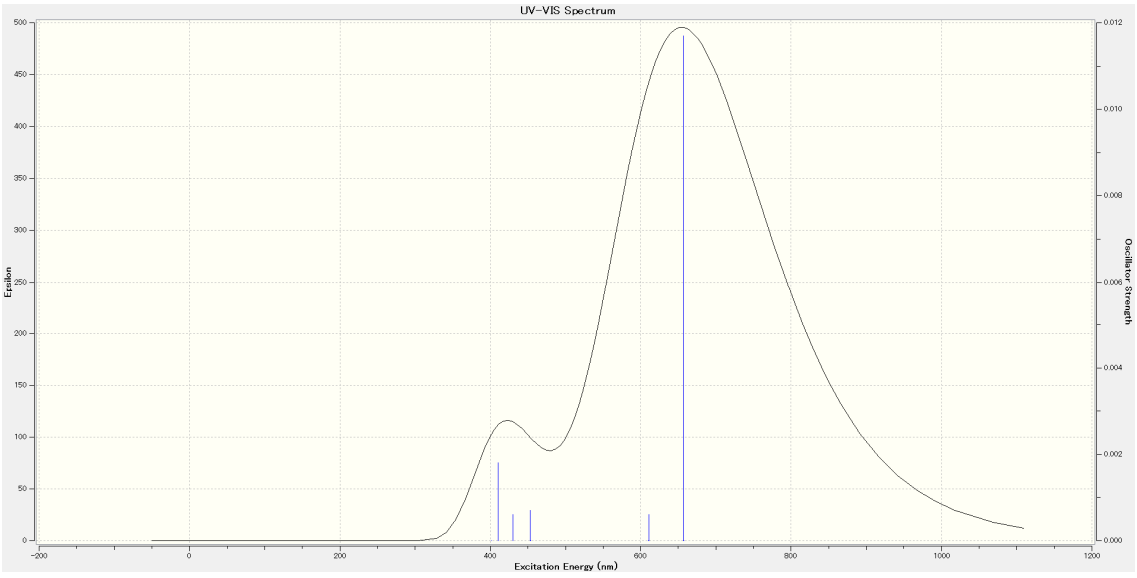

Figure S4. Simulated UV-vis spectrum of free [**113**$^{\cdot}$]$^{-}$ by TD-DFT calculations.

References

(1) (a) Cetinkaya, B.; Hudson, A.; Lappert, M. F.; Goldwhite, H. *J. Chem. Soc., Chem. Commun.* **1982**, 609. (b) Culcasi, M.; Gronchi, G.; Escudié, J.; Couret, C.; Pujol, L.; Tordo, P. *J. Am. Chem. Soc.* **1986**, *108*, 3130. (c) Bard, A. J.; Cowley, A. H.; Kilduff, J. E.; Leland, J. K.; Norman, N. C.; Pakulski, M.; Heath, G. A. *J. Chem. Soc., Dalton Trans.* **1987**, 249. (d) Shah, S.; Burdette, S. C.; Swavey, S.; Urbach, F. L.; Protasiewicz, J. D. *Organometallics* **1997**, *16*, 3395-3400. (e) Dutan, C.; Shah, S.; Smith, R. C.; Choua, S.; Berclaz, T.; Geoffroy, M.; Protasiewicz, J. D. *Inorg. Chem.* **2003**, *42*, 6241. (f) Sasamori, T.; Mieda, E.; Nagahora, N.; Sato, K.; Shiomi, D.; Takui, T.; Hosoi, Y.; Furukawa, Y.; Takagi, N.; Nagase, S.; Tokitoh, N. *J. Am. Chem. Soc.* **2006**, *128*, 12582. (g) Nagahora, N.; Sasamori, T.; Hosoi, Y.; Furukawa, Y.; Tokitoh, N.; *J. Organomet. Chem.* **2008**, *693*, 625.

(2) (a) Binder, H.; Riegel, B.; Heckmann, G.; Moscherosch, M.; Kaim, W.; von Schnering, H. -G.; Hönle, W.; Flad, H.-J.; Savin, A. *Inorg. Chem.* **1996,** *35*, 2119. (b) Geier, J.; Harmer, J.; Grützmacher, H. *Angew. Chem. Int. Ed*. **2004,** *43*, 4093.

(3) Back, O.; Donnadieu, B.; von Hopffgarten, M.; Klein, S.; Tonner, R.; Frenking, G.; Bertrand, G. *Chem. Sci.* **2011,** *2*, 858.

(4) (a) Bartlett, R. A.; Feng, X.; Power, P. P. *J. Am. Chem. Soc.* **1986**, *108*, 6817. (b) Doris, C. P.; Philip, P. P. *J. Am. Chem. Soc.* **1991**, *113*, 8426.

(5) Asami, S.-s.; Okamoto, M.; Suzuki, K.; Yamashita, M. *Angew. Chem. Int. Ed.* **2016,** *55*, 12827-12831.

(6) Urnéžius, E.; Protasiewicz, J. D. *Main Group Chem.* **1996**, *1*, 369.

(7) Sasamori, T.; Takeda, N.; Tokitoh, N. *J. Phys. Org. Chem.* **2003**, *16*, 450.

(8) Emsley, J.; *The Elements*, 3rd ed.; Oxford University Press: New York. 1998.

(9) The optimized structure of the contact ion pair [**113**$^{\cdot}$]$^{-}$[K(THF)$_2$]$^{+}$ is similar to the free anion [**113**$^{\cdot}$]$^{-}$ derived from [**113**$^{\cdot}$]$^{-}$[K(THF)$_2$]$^{+}$. The optimization of the anionic part of [**113**$^{\cdot}$]$^{-}$[K(cryptand)]$^{+}$ also generated the free anion with a similar structure and a slightly higher energy (0.23 kcal/mol). The discussion herein is therefore based on the free anion that was obtained from the optimization of [**113**$^{\cdot}$]$^{-}$[K(THF)$_2$]$^{+}$.

(10) Catheline, A.; Valles, C.; Drummond, C.; Ortolani, L.; Morandi, V.; Marcaccio, M.; Iurlo, M.; Paolucci, F.; Penicaud, A. *Chem. Commun.* **2011,** *47*, 5470.

(11) Kabuto, C.; Akine, S.; Kwon, E., *J. Cryst. Soc. Jpn.* **2009,** *51*, 218.

(12) (a) Altomare, A.; Burla, M. C.; Camalli, M.; Cascarano, G. L.; Giacovazzo, C.; Guagliardi, A.; Moliterni, A. G. G.; Polidori, G.; Spagna, R., *J. Appl. Crystallogr.* **1999,** *32*, 115. (b) Burla, M. C.; Caliandro, R.; Camalli, M.; Carrozzini, B.; Cascarano, G. L.; De Caro, L.; Giacovazzo, C.; Polidori, G.; Spagna, R. *J. Appl. Crystallogr.* **2005,** *38*, 381. (c) Burla, M. C.; Caliandro, R.; Carrozzini, B.; Cascarano, G. L.; Cuocci, C.; Giacovazzo, C.; Mallamo, M.; Mazzone, A.; Polidori, G. *J. Appl. Crystallogr.* **2015,** *48*, 306.

(13) (a) Sheldrick, G. M. *SHELXL-97, Program for the Refinement of Crystal Structures*, University of Göttingen: Göttingen, Germany, 1997. (b) Sheldrick, G. *Act. Cryst. Sec. C* **2015,** *71*, 3.

(14) (a) Lee, C.; Yang, W.; Parr, R. G. *Phys. Rev. B* **1988**, *37*, 785. (b) Becke, A. D. *Phys. Rev. A* **1988**, *38*, 3098-3100; (c) Miehlich, B.; Savin, A.; Stoll, H.; Preuss, H. *Chem. Phys. Lett.* **1989**, *157*, 200. (d) Becke, A. D. *J. Chem. Phys.* **1993**, *98*, 5648. (e) Stephens, P. J.; Devlin, F. J.; Chabalowski, C. F.; Frisch, M. J. *J. Phys. Chem.* **1994**, *98*, 11623.

(15) Huzinaga, S.; Andzelm, J.; Klobukowski, M. R.-A.; Esakai, Y.; Tatewaki, H. *Gaussian basis sets for molecular calculations*, Elsevier, **1984**.
(16) Frisch, M. J.; Trucks, G. W.; Schlegel, H. B.; Scuseria, G. E.; Robb, M. A.; Cheeseman, J. R.; Scalmani, G.; Barone, V.; Mennucci, B.; Petersson, G. A.; Nakatsuji, H.; Caricato, M.; Li, X.; Hratchian, H. P.; Izmaylov, A. F.; Bloino, J.; Zheng, G.; Sonnenberg, J. L.; Hada, M.; Ehara, M.; Toyota, K.; Fukuda, R.; Hasegawa, J.; Ishida, M.; Nakajima, T.; Honda, Y.; Kitao, O.; Nakai, H.; Vreven, T.; Montgomery Jr, J. A.; Peralta, J. E.; Ogliaro, F.; Bearpark, M. J.; Heyd, J.; Brothers, E. N.; Kudin, K. N.; Staroverov, V. N.; Kobayashi, R.; Normand, J.; Raghavachari, K.; Rendell, A. P.; Burant, J. C.; Iyengar, S. S.; Tomasi, J.; Cossi, M.; Rega, N.; Millam, N. J.; Klene, M.; Knox, J. E.; Cross, J. B.; Bakken, V.; Adamo, C.; Jaramillo, J.; Gomperts, R.; Stratmann, R. E.; Yazyev, O.; Austin, A. J.; Cammi, R.; Pomelli, C.; Ochterski, J. W.; Martin, R. L.; Morokuma, K.; Zakrzewski, V. G.; Voth, G. A.; Salvador, P.; Dannenberg, J. J.; Dapprich, S.; Daniels, A. D.; Farkas, Ö.; Foresman, J. B.; Ortiz, J. V.; Cioslowski, J.; Fox, D. J. *Gaussian09, Revision D.01*. Gaussian, Inc.: Wallingford, CT, USA, 2013.
(17) Reed, A. E.; Curtiss, L. A.; Weinhold, F. *Chem. Rev.* **1988**, *88*, 899.

Chapter 4

Two-Electron Reduction of Diboryldiphosphene: Formation of Intramolecular Charge Transfer Complex of Dianionic B=P–P=B Species

4-1, Introduction

The author has already mentioned about 1,3-butadiene derivatives including heavier elements (chapter 1.13). Although boryl substituents have π accepter properties due to the vacant p-orbital on boron, 1,4-diboranuida-2,3-diphosphabutadiene have never been reported. In addition, related compound of 1,2-boryldiphosphane have been considered not to show 1,4-diboranuida-2,3-diphosphabutadiene structure, because of large dihedral angles of each phosphorus containing planes [Figure 1 (a)].[1] (av 70.5º)

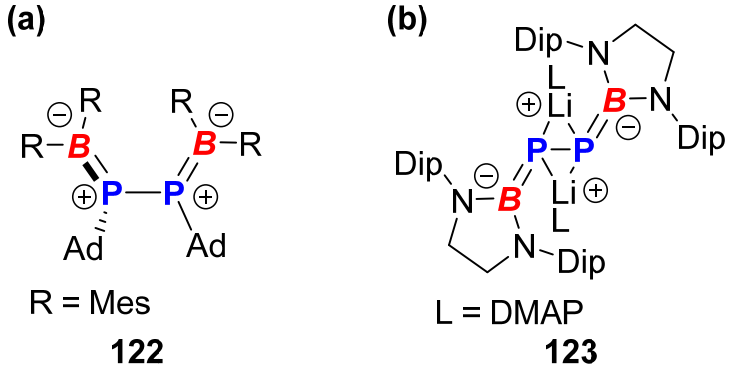

Figure 1. Structures of (a) 1,2-diboryldiphosphane and (b) boryl-substituted diphosphanediide **123**·[DMAP]$_2$

Redox properties of diphosphene, P=P double bond species, have been initiated by the first discovery of Mes*-diphosphene by Yoshifuji.[2] For example, diphosphenes could be reversibly reduced to the corresponding radical anions, which were characterized by ESR spectroscopy but not isolated until recently.[3] In contrast, doubly reduced diphosphene dianion has never been reported. Considering that the π-accepting effect of boryl substituent could stabilize anionic phosphide through pπ-pπ interaction between B and P,[4] one can expect that these reduced diphosphene radical anion and dianion would be stabilized by introduction of boryl substituents. In facts, we recently reported the isolation and structural characterization of a boryl-substituted diphosphene **113** and its radical anion by utilizing the π-acceptor property of boryl substituent.[5] Herein, the author reports the synthesis and properties of boryl-substituted diphosphanediide **123** as a doubly reduced diphosphene and its DMAP adduct **123**·[DMAP]$_2$. X-ray diffraction analysis, NMR and UV-vis spectroscopy, and DFT calculations revealed the latter compound possesses 1,4-diboranuda-2,3-diphosphabutadiene (B^-=P–P=B^-) character over two consecutive B=P double bonds.

4-2, Results and discussions

4-2-1, Synthesis of diphosphanediide 123 and 123·[DMAP]$_2$

The previously reported diboryldiphosphene **113**[6] was reduced by treatment with an excess amount of lithium in toluene to afford mainly boryl-substituted diphosphanediide **123** as orange solids (Scheme 1). In the ^{31}P NMR spectrum of **123** in C_6D_6, two magnetically equivalent phosphorus nuclei resonated at -307 ppm, which is upfield shifted in comparison with those of the previously reported diphosphanediide (–106 to –24ppm).[6] Additionally, the ^{7}Li NMR signal of **123** in C_6D_6 has exhibited a triplet signal at -0.15 ppm with $^1J_{PLi}$ of 30 Hz, because of interaction between lithium and two phosphorus nuclei. The ^{11}B NMR spectra of the dianionic **123** showed a broad singlet at 37 ppm, which is slightly shifted to lower field in comparison with that of **113** (31 ppm), as a negative change on the boron center with sp^2 hybridization does not affect the ^{11}B NMR chemical shift. Although

the author could not isolate **123** completely due to a small amount of byproducts, reactivity of **123** as diphosphanediide was confirmed by a reaction with MeI in toluene. As a result 1,2-diboryl-1,2-dimethyldiphosphane **124** was obtained as a the sole product (isolation yield 46%: NMR yield 78% from **113**) and the structure of **124** was also supported by preliminary X-ray diffraction analysis, showing a singlet signal in the ^{31}P NMR spectroscopy (δ_p -124.9). In addition, these results have shown that almost diphosphene **113** was transformed into diphosphanediide **123** by two electron reduction. **123**·$[DMAP]_2$ has been isolated by recrystallization from 1.5 eq DMAP and hexane/toluene solution. **123**·$[DMAP]_2$ led to a downfield shift of phosphorus signal at δ_p -267 ppm in comparison with **123** (δ_p -307 ppm). Reflecting the coordination to Li, downfield shift of all aromatic protons in DMAP has been confirmed by ^{1}H NMR spectrum. A triplet signal at 1.5 ppm in ^{7}Li NMR spectrum of **123**·$[DMAP]_2$ was observed with a smaller coupling constant of 25 Hz than that of **123** to indicate the interaction between Li and P nuclei was weakened upon coordination of DMAP. The ^{11}B NMR chemical shift of **123**·$[DMAP]_2$ was similar to that of **123**.

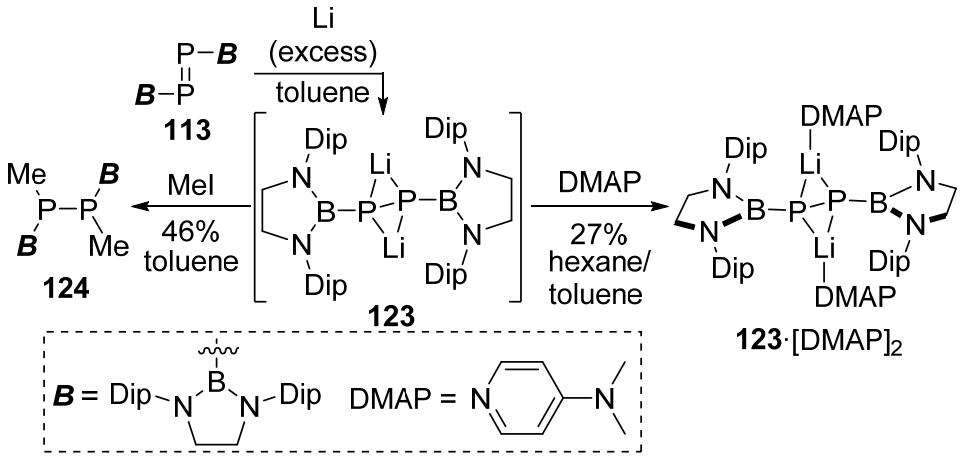

Scheme 1 Synthesis of boryl-substituted diphosphanediide **123** and 1,2-diboryl-1, 2-dimethydiphosphine **124**
Unfortunately, the author comfirmed generation of byproduct (δ_P -222) by using some other ligands, which were DME, TMEDA, and 12-crown-4-ether.

4-2-2, X-ray structure **123** and **123**·$[DMAP]_2$

The centrosymmetric molecular structure of **123** was determined by single-crystal X-ray diffraction analysis (Figure 2). In the crystal, Li atoms bridged two phosphorus atoms to form a contact ion pair with four identical P-Li bond of 2.452(7) Å. The observed P–P bond length of 2.2723(16) Å is slightly longer than the typical P–P single bond (~2.2 Å) and that of monomeric diphosphanediide [2.244 Å].[7] The B1–P1 bond lengths of 1.930(3) Å in **123** are similar to the B–P bond length of **113** [1.936(3) Å], indicating its single-bond character. The B1–P1–P1* angle of 90.83(10)° in **123** is narrower than that of 95.83(9)° in **113**. The two boron-containing planes are oriented almost perpendicular to the planar BPPB moiety [P1*–P1–B1–N2: 92.16°]. Thus, anionic charges on each phosphorus atom in **123** were used for the interaction with two Li cations. In contrast to the case of **123**, single-crystal X-ray diffraction analysis on **123**·$[DMAP]_2$ suggested the existence of pπ-pπ interactions between the anionic phosphorus atom and the adjacent boron atom (Figure 3). Although P–P bond length of 2.2761(11) Å and the P-Li bond lengths [2.46(2) and 2.49(2) Å: Li atom was disordered] in **123**·$[DMAP]_2$ are similar to

those of **123**, the P-B bond length of 1.899(2) Å are remarkably shorter than those of **123** [1.930(3) Å]. Moreover, the boron-containing planes in **123**·$[DMAP]_2$ adopt an almost coplanar orientation with respect to the planar BPPB moiety [P1*–P1–B1–N2: 171.73(13)°]. Thus, the anionic core has a character of two consecutive P=B double bonds.

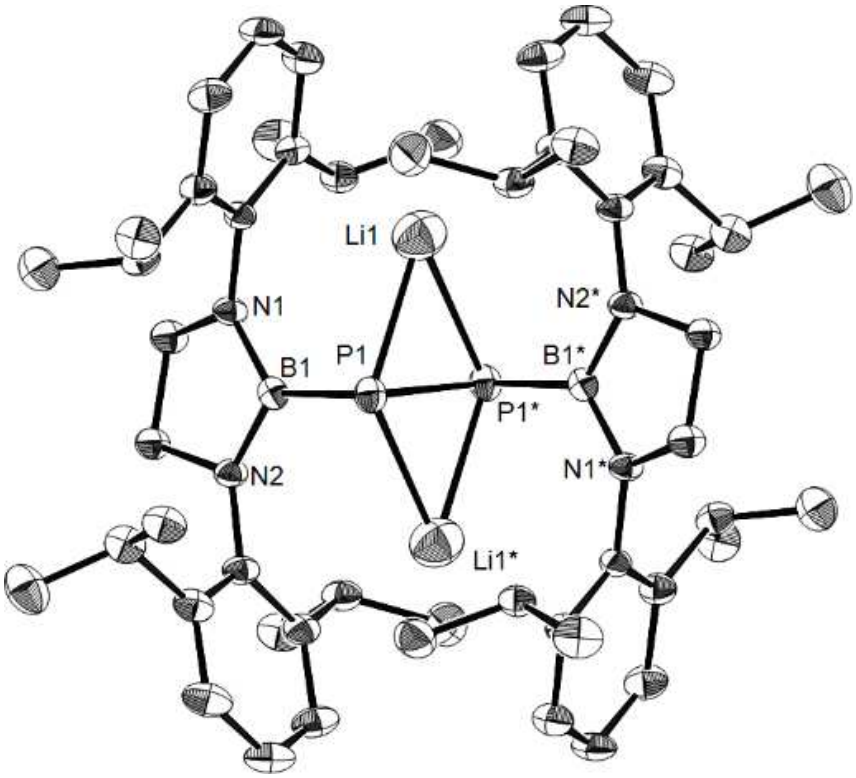

Figure 3. Molecular structure of **123** (thermal ellipsoids set at 50% probability, hydrogen atoms are omitted for clarity; asterisks denote atoms generated by symmetry operation), Selected bond lengths [Å] and angles [°]: P1-B1 1.930(3), N1-B1 1.423(4), N2-B1 1.429(4), P1-P1* 2.2723(16), P1*-P1-B1 90.83(10), N1-B1-N2 106.7(2), P1*-P1-B1-N2 92.16, P1-Li1 2.452(7)

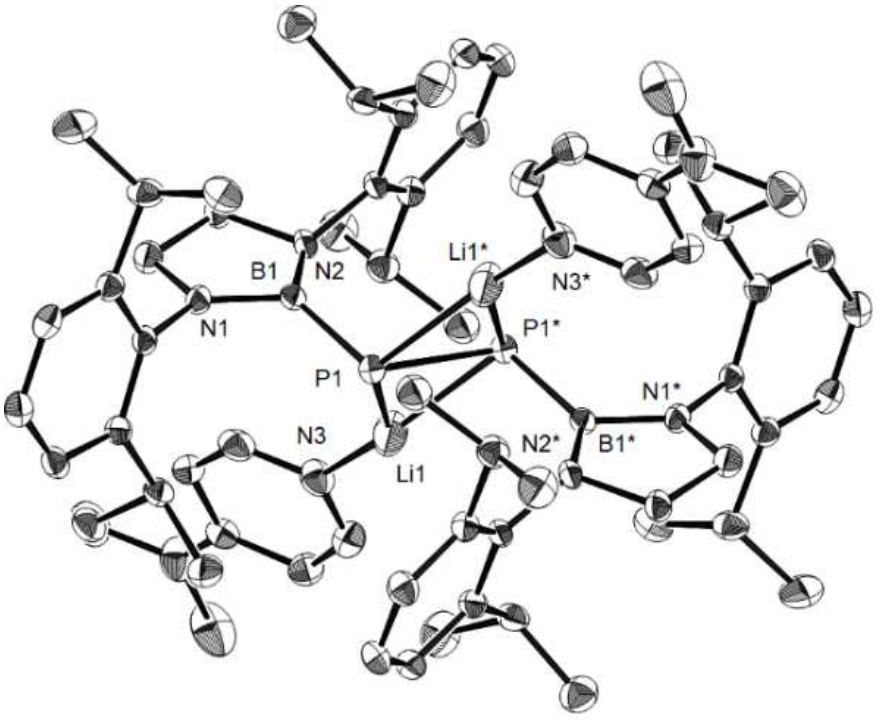

Figure 4. Molecular structure of **123**·$[DMAP]_2$ (thermal ellipsoids set at 50% probability, hydrogen atoms, minor parts of disordered Li atoms, and co-crystallized toluene molecules are omitted for clarity; asterisks denote atoms generated by symmetry operation), Selected bond lengths [Å] and angles [°]: P1-B1 1.899(2), N1-B1 1.442(2), N2-B1 1.464(2), P1-P1* 2.2761(11), P1*-P1-B1 102.49(7), N1-B1-N2 105.96(15), P1*-P1-B1-N2 171.73(13), P1-Li1 2.46(2)

4-2-3, DFT calculations of diphosphanediide 123 and 123·$[DMAP]_2$

DFT calculations at the B3LYP/6-31G(d) level of theory revealed characteristic molecular orbitals of **123** and **123**·$[DMAP]_2$ (Figure 5). In both **123** and **123**·$[DMAP]_2$, HOMO, HOMO-1, and HOMO-4 showed similar symmetry to π*-orbital, lone pairs on P atoms, and π-orbitals of **113**, although P–P bond in **123** and **123**·$[DMAP]_2$ exhibited no double bond character as judged by the bond length. LUMO of **123** is considered as π*-orbitals of the Dip rings, while LUMO of **123**·$[DMAP]_2$ corresponds to π*-orbitals of coordinating DMAP ligands to Li. It should be noted that LUMO+1 of **123**·$[DMAP]_2$ has exactly similar shape to that of LUMO and is almost degenerated with LUMO considering their similar energy levels. As observed in crystal structure, HOMO of **123**·$[DMAP]_2$ exhibited B^-=P-P=B^- π-bond character, while HOMO of **123** exhibited no contribution of π-accepting character of boryl substituents due to the orthogonal relationship between the boron planes and the P=P moiety. The Wiberg bond indexes of **123**·$[DMAP]_2$ (P-B: 1.27, P-P: 0.987) also supported that existence of pπ-pπ interaction between P and B atoms and P–P single bond character. An NBO analysis of **123**·$[DMAP]_2$ suggested that donor-acceptor interactions exist between P and B atoms [second-order perturbation energy, P to B: 49.56 kcal/mol, N to B: 53.76 kcal/mol (av.)]. These interactions between P and B atoms in **123**·$[DMAP]_2$ are larger than those in the previously reported radical anion of **113** [29.61 kcal/mol (av.)].[4] Thus, **123**·$[DMAP]_2$ can be described with the resonance structures in Scheme 2, involving a contribution of 1,4-diboranuida-2,3-diphosphabutadiene[8] structure.

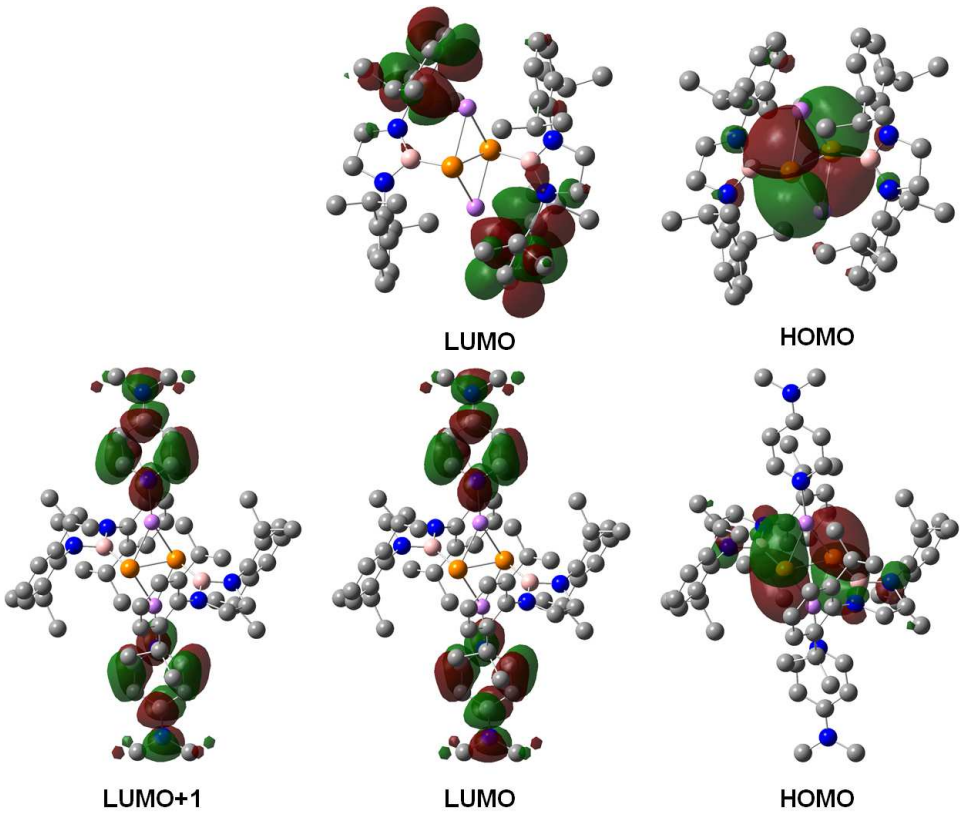

Figure 5. Kohn-Sham orbitals of **123** (top) and **123**·[DMAP]$_2$ (bottom) calculated at the B3LYP/6-31G(d) level of theory (hydrogen atoms are omitted for clarity, gray: carbon, blue: nitrogen, orange: phosphorus, pale peach: boron, purple: lithium)

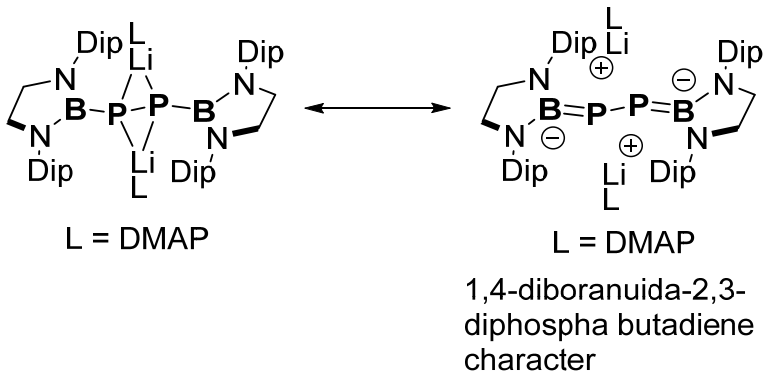

Scheme 2. Resonance structure of **123**·[DMAP]$_2$

4-2-4, UV-spectrum of 123 [DMAP]$_2$

The coexistence of the dianionic B^-=P-P=B^- moiety and aromatic rings of the Li-coordinated DMAPs induced an intermolecular charge transfer absorption. In fact, the UV-vis spectrum of **123**·[DMAP]$_2$ (Figure 6) showed a characteristic absorption maximum at 380 nm (ε 3660), which was assigned as a transition from HOMO (π-orbital of B^-=P-P=B^- moiety) to LUMO+1 (π^*-orbital of DMAP) by TD-DFT calculations. This absorption was slightly weaker and red-shifted in comparison with that of 2,3-diphosphabutadiene derivative possessing Mes*

and $OSiMe_3$ substituents (370 nm, ε 20400).[9] It should be noted that the absorption edge reaches to ca. 650 nm, which is further longer than that expected for absorption maximum. One can expect that the degenerated LUMO+1 would contribute to longer-wavelength absorption even its oscillator strength is weak. Furthermore, the energy levels of molecular orbitals in anionic species could be sensitive to the counter cations and their conditions. In fact, complexation of DMAP to Li in **123**·$[DMAP]_2$ induced higher HOMO and lower LUMO levels in comparison with those of **123** (Figure **7**), as a similar effect of counter cation toward MO levels was observed for dianionic 1,2-diborin derivatives. An additionally observed absorption maximum of **123**·$[DMAP]_2$ at 303 nm was also characterized as a transition from HOMO to LUMO+3 (π*-orbitals of Dip rings).

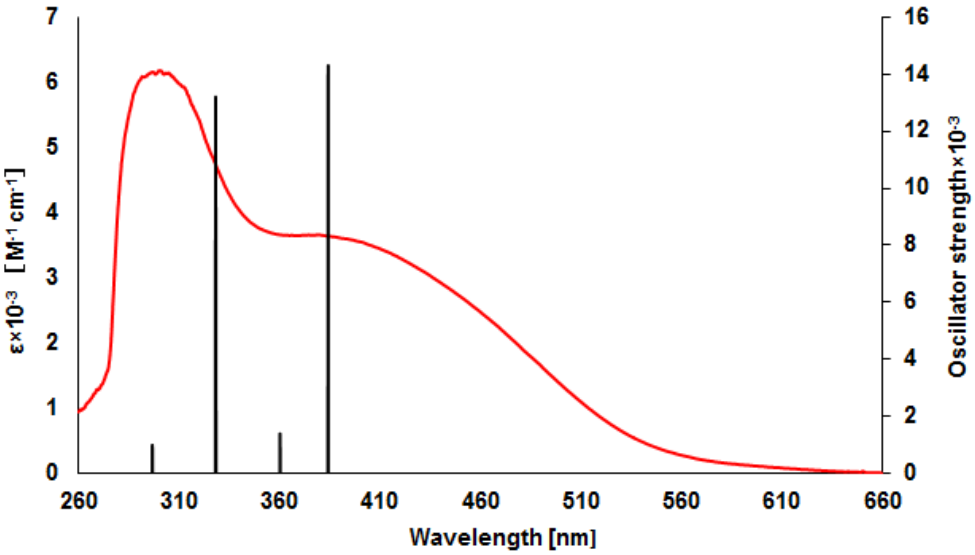

Figure 6. UV-vis spectra of **123**·$[DMAP]_2$ (red) in toluene (500 μM) at room temperature, together with calculated transitions (black) at the CAM-B3LYP/6-31G(d) level of theory.

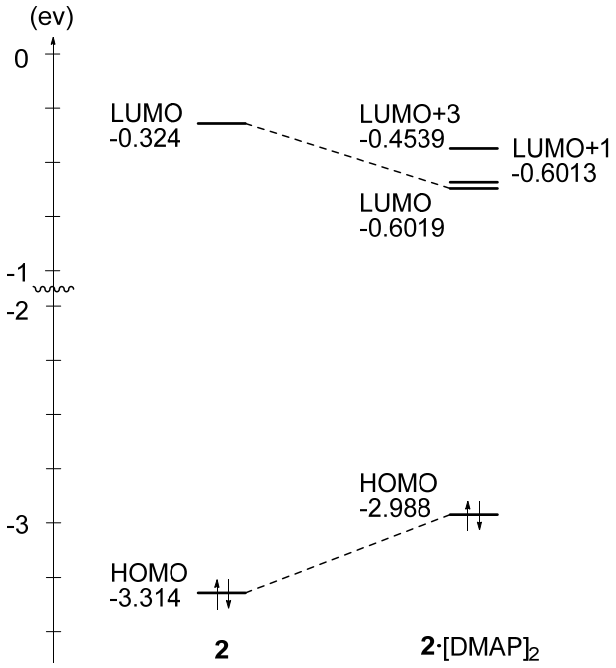

Figure 7. Energy diagrams for molecular orbitals of **123** and **123**·$[DMAP]_2$ calculated at the B3LYP/6-31G(d) level of theory

4-3, Conclusion

Boryl-substituted diphosphene **113** was reduced with two electrons by treatment with Li to form diboryldiphosphanediide **123**. Reaction of **123** with MeI resulted in the formation of 1,2-diboryl-1,2-dimethyldiphosphane **124**. Coordination of DMAP to **123** led to the formation of **123**·$[DMAP]_2$, X-ray crystallographic analysis and DFT calculations revealed that the coordination of DMAP to **123** induced significant pπ-pπ interaction between P and B atoms. UV-vis spectrum of **123**·$[DMAP]_2$ exhibited a characteristic abosorption at 380 nm which was assigned as an intramolecular charge transfer by TD-DFT calculations.

Experimental procedure

General procedures

All manipulations involving the air- and moisture-sensitive compounds were carried out in a glovebox (Miwa MFG and Korea KIYON) under argon. Toluene and *n*-hexane were purified by passing through a solvent purification system (Grass Contour). Lithium dispersion (purchased from Kanto Chemical Co., Inc., containing 1% sodium) was washed with hexane before the use to make a lithium powder. NMR spectra were recorded on 500 or 400 MHz spectrometers. Chemical shifts are reported in ppm relative to the residual partially protonated solvent for ^{1}H, deuterated solvent for ^{13}C, external $BF_3 \cdot OEt_2$ for ^{11}B, and 85% H_3PO_4 for ^{31}P nuclei. Data are presented in the following manner: chemical shift, multiplicity (s = singlet, d = doublet, t = triplet, sept = septet, m = multiplet, br = broad, brs = broad singlet), coupling constant in hertz (Hz), and signal area integration in natural numbers. Mass spectra were measured on a JEOL JMS-700 mass spectrometer. Melting points were determined on Optimelt (SRS) and were uncorrected. X-ray crystallographic analysis was performed on VariMax/Saturn CCD diffractometer. UV/vis spectrum was recorded on DT-MINI-2-GS (Ocean Optics). Boryl-substituted diphosphene **113** was synthesized according to the literature procedure.[5]

Synthesis of 123

In a glovebox, toluene (7.8 mL) was added to a mixture of **113** (90.0 mg, 107 μmol) and Li powder (74.0 mg, 10.7 mmol) in a 30 mL vial at room temperature. The color of the resulting solution rapidly turned into red. After the reaction mixture was stirred at room temperature for 2 h, the resulting suspension was filtered through a pad of Celite® to remove an excess amount of Li powder. The solvent was removed under reduced pressure to give orange solids of **123** (90.5 mg, ca. 106 μmol, 99 %) containing a small amount of byproduct. Single crystals suitable for X-ray analysis were obtained from Et_2O and hexane. ^{1}H NMR (C_6D_6, 500 MHz) δ 1.17 (d, *J* = 7 Hz, 24H), 1.33 (d, *J* = 7 Hz, 24H), 3.58 (sep, *J* = 7 Hz, 8H), 3.58 (s), 7.01 (d, *J* = 8 Hz, 8H), 7.10 (t, *J* = 8 Hz, 4H); ^{11}B NMR (toluene, 160 MHz) δ 39 (br s); ^{31}P NMR (toluene, 202 MHz) δ –307 (s); ^{7}Li NMR (C_6D_6, 194 MHz) δ –0.15 (t, *J* = 28 Hz) ; HRMS (FAB^+) *m/z* Calcd. for $C_{52}H_{78}B_2N_4P_2$ $[M+2H]^+$ 842.5885, found; 842.5898.

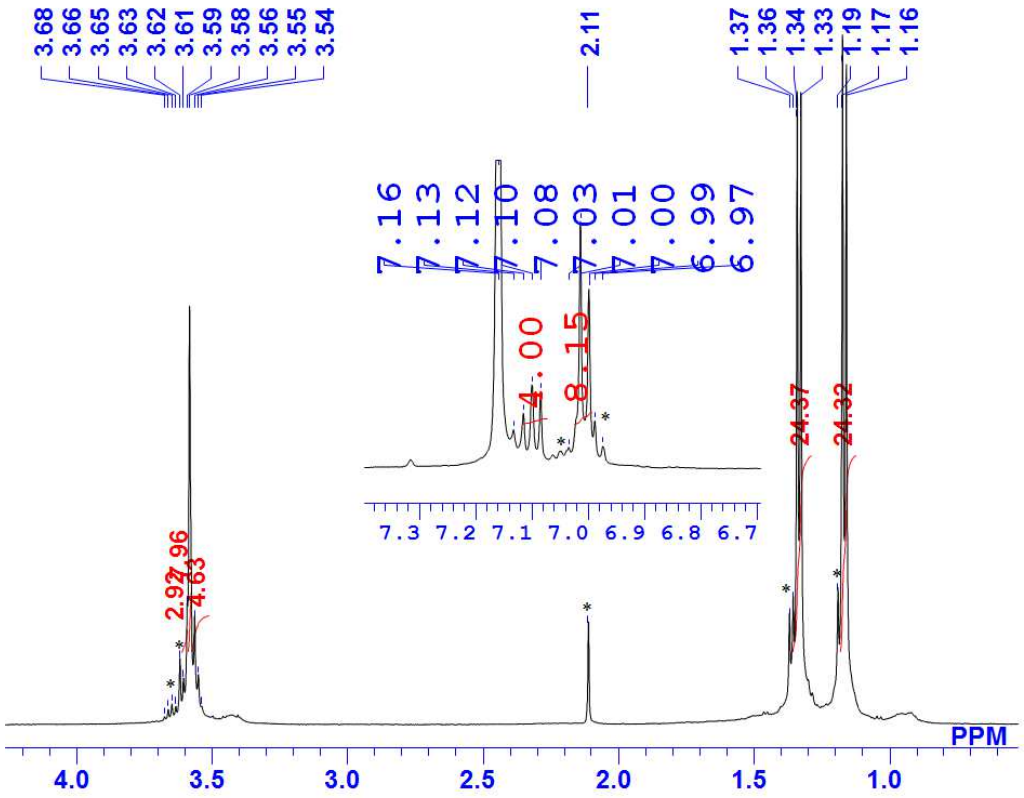

Figure S1. ^{1}H NMR spectrum of **123** (* denotes signal of the impurity)

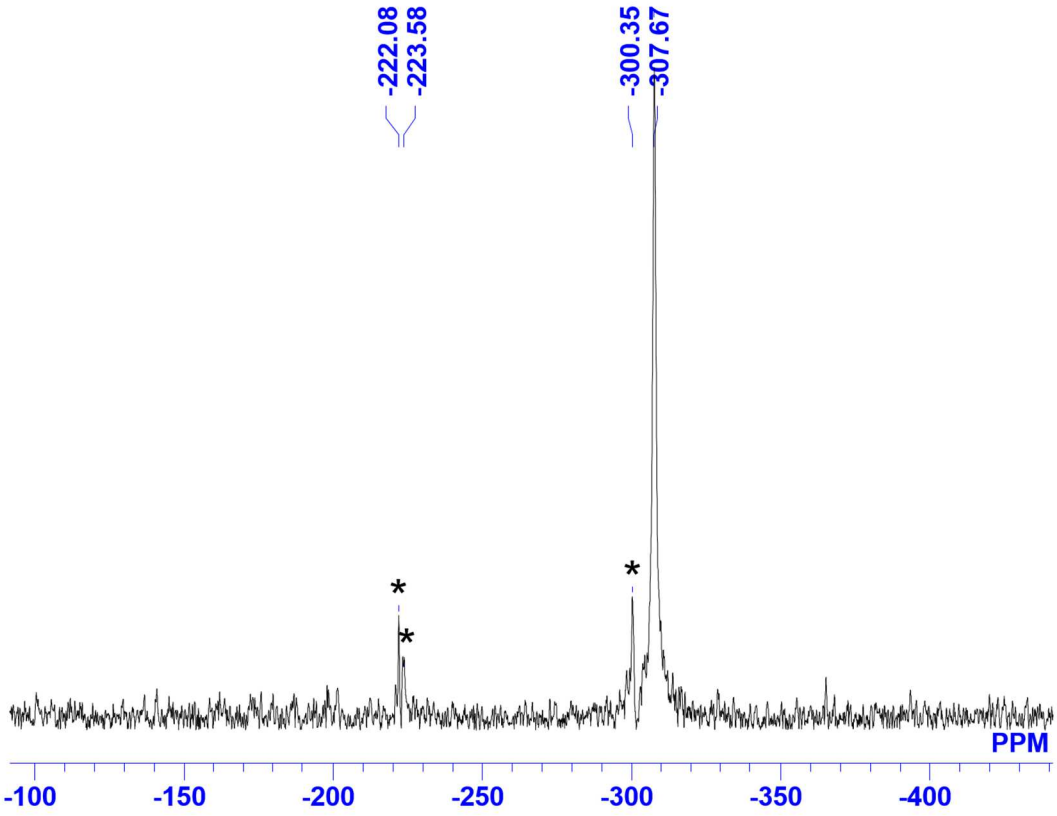

Figure S2. ^{31}P NMR spectrum of **123** (* denotes signal of the impurity)

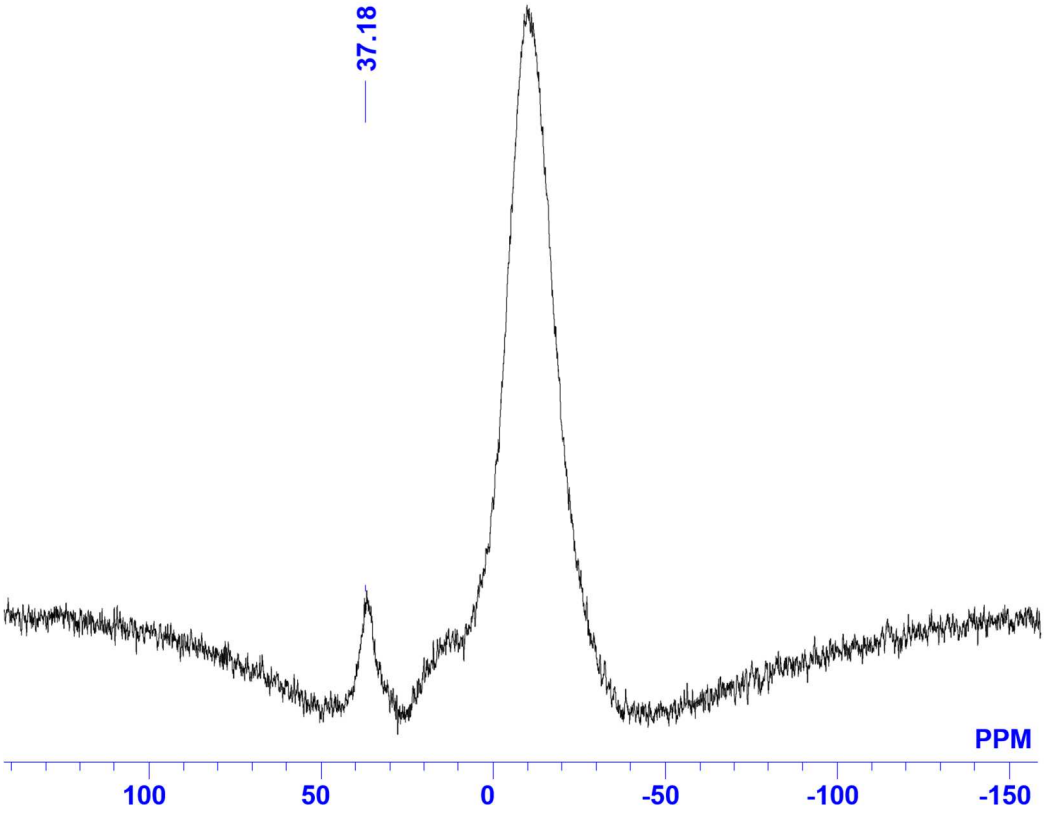

Figure S3. ^{11}B NMR spectrum of **123**

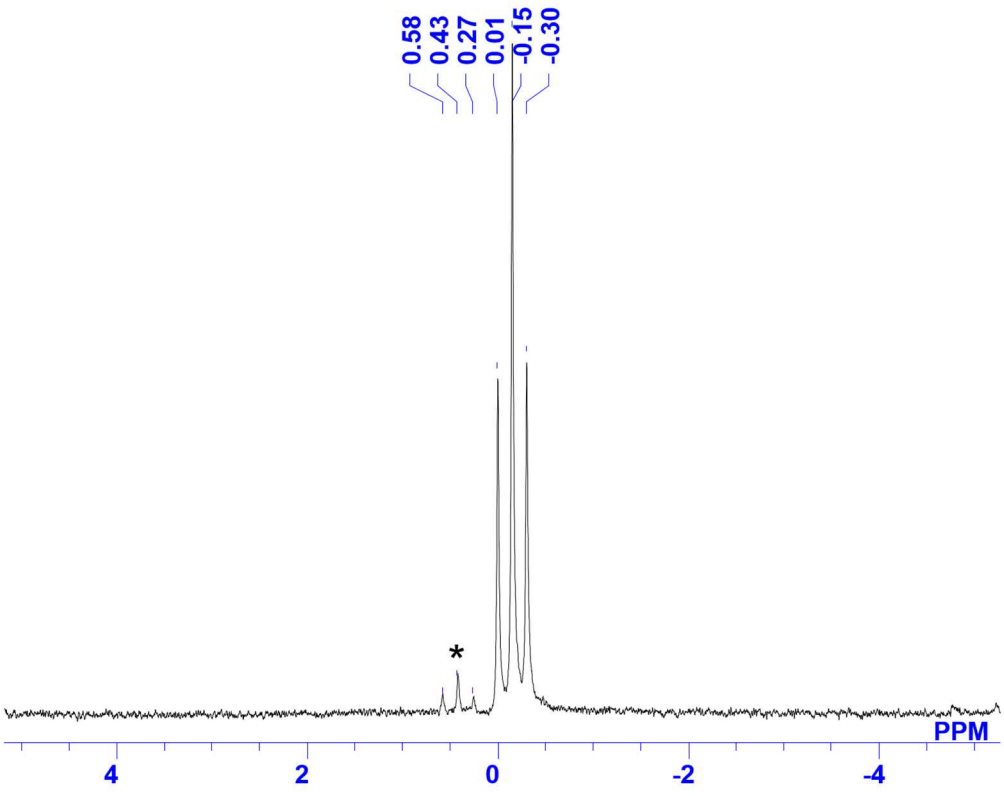

Figure S4. ^{7}Li NMR spectrum of **123** (* denotes signal of the impurity)

Synthesis of 123·[DMAP]$_2$

In a glovebox, toluene (7.8 mL) was added to a mixture of **113** (90.0 mg, 107 μmol) and Li powder (74.0 mg, 10.7 mmol) in a 30 mL vial at room temperature. The color of the resulting solution rapidly turned into red. After the reaction mixture was stirred at room temperature for 6 h, the resulting suspension was filtered through a pad of Celite® to remove an excess amount of Li powder. After removal of the volatiles from the filtrate, the residue was recrystallized from a mixture of hexane and toluene in the presence of DMAP (19.6 mg, 0.161 μmol, 1.5 equiv. to **113**) to give brown crystals of **123**·[DMAP]$_2$ (32.0 mg, 27%).

^{1}H NMR (C_6D_6, 500 MHz) δ 1.26 (d, *J* = 7 Hz, 24H), 1.33 (d, *J* = 7 Hz, 24H), 2.21 (s, 12H), 3.61 (s, 8H), 3.76 (sep, *J* = 7 Hz, 8H), 6.12 (d, *J* = 5 Hz, 4H), 7.14 (d, *J* = 8 Hz, 8H), 7.22 (t, *J* = 8 Hz, 4H), 8.14 (br s) ^{11}B NMR (C_6D_6, 160 MHz) δ 37 (br s); ^{31}P NMR (C_6D_6, 202 MHz) δ –267 (s); ^{7}Li NMR (C_6D_6, 194 MHz) δ 1.54 (t, *J* = 24 Hz); mp: 146.7-168.6 ºC; HRMS (FAB$^+$) *m/z* Calcd. for $C_{52}H_{78}B_2N_4P_2$ [M–2Li–DMAP+2H]$^+$ 842.5893, found; 842.5963.

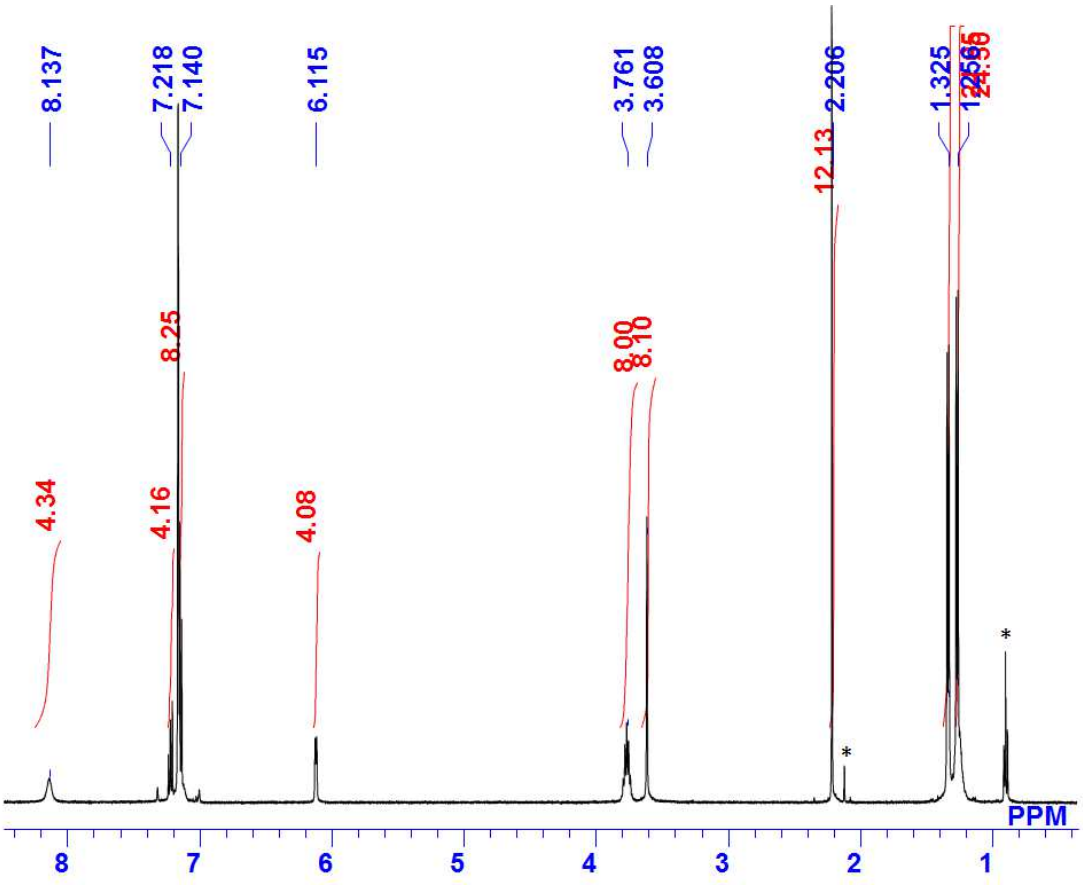

Figure S5. ^{1}H NMR spectrum of **123**·[DMAP]$_2$ (* denotes signal of *n*-hexane and toluene)

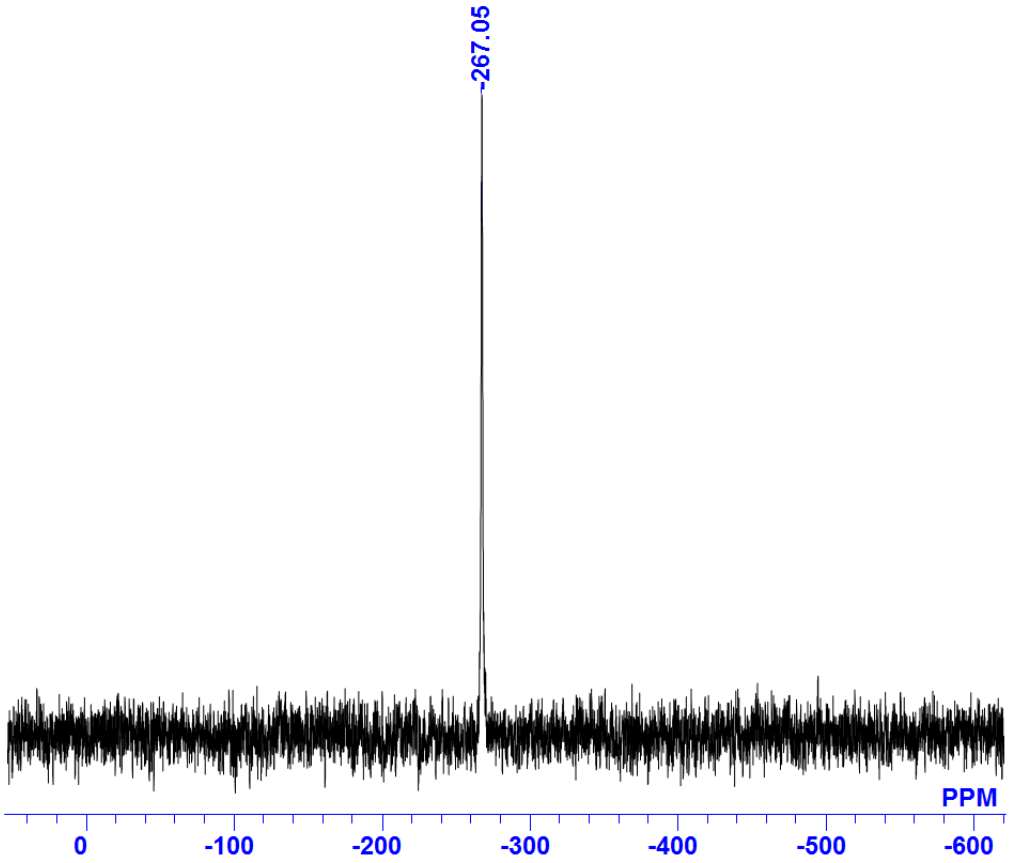

Figure S6. ^{31}P NMR spectrum of **123**·[DMAP]$_2$

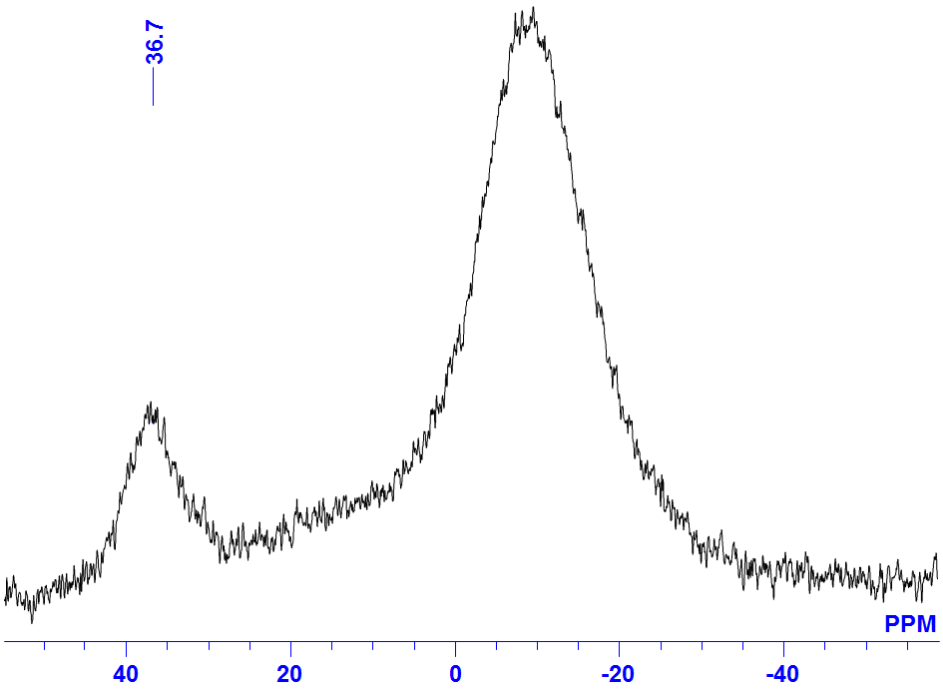

Figure S7. ^{11}B NMR spectrum of **123**·[DMAP]$_2$

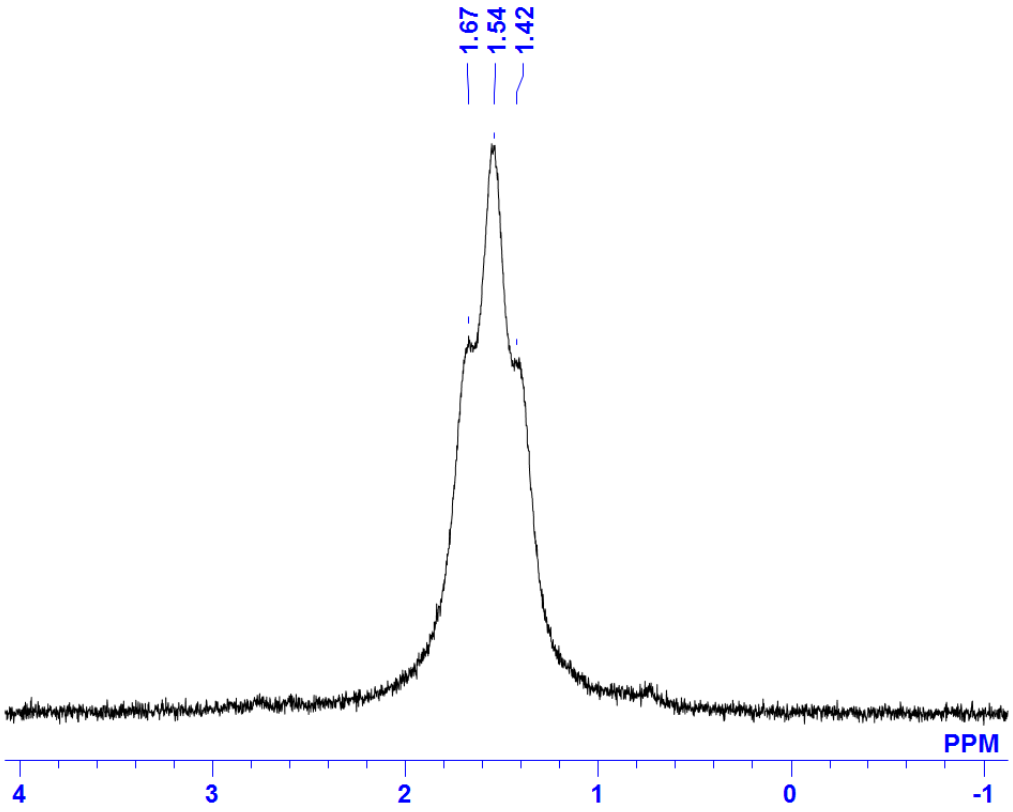

Figure S8. ^{7}Li NMR spectrum of **123**·[DMAP]$_2$

Synthesis of 3

In a glovebox, toluene (10 mL) was added to a mixture of **113** (80.0 mg, 95.2 μmol) and Li powder (66.0 mg, 9.52 mmol) in a 30 mL vial. The color of the resulting solution rapidly turned into red. After the reaction mixture was stirred at room temperature for 5 h, the resulting suspension was filtered through a pad of Celite® to remove an excess amount of Li powder. The resulting mixture was added dropwise to a toluene solution (3 mL) of MeI (35.6 μL, 0.571 mmol) in 30 mL vial. The resulting suspension was filtered through a pad of Celite® to remove insoluble salts, the residue was purified by recrystallization with hexane to give colorless crystals of **124** (39.5 mg, 46 %). ^{1}H NMR (C_6D_6, 400 MHz) δ 0.78 (vt, *J* = 3 Hz, 6H, Although the reason why this signal resonates as a triplet is not clear so far, we tentatively assigned this signal as a virtual triplet because PhMeP-PMePh was also found to exhibit similar triplet signal in the following reference: Schneider, H.; Schmidt, D.; Radius, U. *Chem. Commun.* **2015,** *51*, 10138-10141.), 1.07 (d, *J* = 7 Hz, 12H), 1.17 (d, *J* = 7 Hz, 12H), 1.22 (d, *J* = 7 Hz, 12H), 1.41 (d, *J* = 7 Hz, 12H), 3.41 (s, 8H), 3.46 (sep, *J* = 7 Hz, 4H), 3.50 (sep, *J* = 7 Hz, 4H), 7.03 (dd, *J* = 7, 2 Hz, 4H); 7.09 (dd, *J* = 8, 2 Hz, 4H); 7.17 (t, *J* = 8 Hz, 4H); ^{13}C NMR (C_6D_6, 125 MHz) δ 4.07 (t, *J* = 12 Hz, P*CH*$_3$), 23.7 (t, *J* = 3 Hz, CH_3), 24.13 (CH_3), 26.42 (CH_3), 26.70 (CH_3), 28.37 (CH_3), 28.55 (CH_3), 54.95 (CH_2), 123.78 (CH), 124.02 (CH), 126.91 (CH), 140.97 (4°), 146.99 (4°), 147.21 (4°); ^{11}B NMR (C6D6, 160 MHz) δ 31 (br s), ^{31}P NMR (C_6D_6, 194 MHz) 125 (s), mp: 293.4-309.1 ºC (decomp); HRMS (ESI$^+$) *m/z* Calcd. for [$C_{54}H_{82}{}^{11}B^{10}BN_4P_2$] (M+) 869.6233, found; 869.6217.

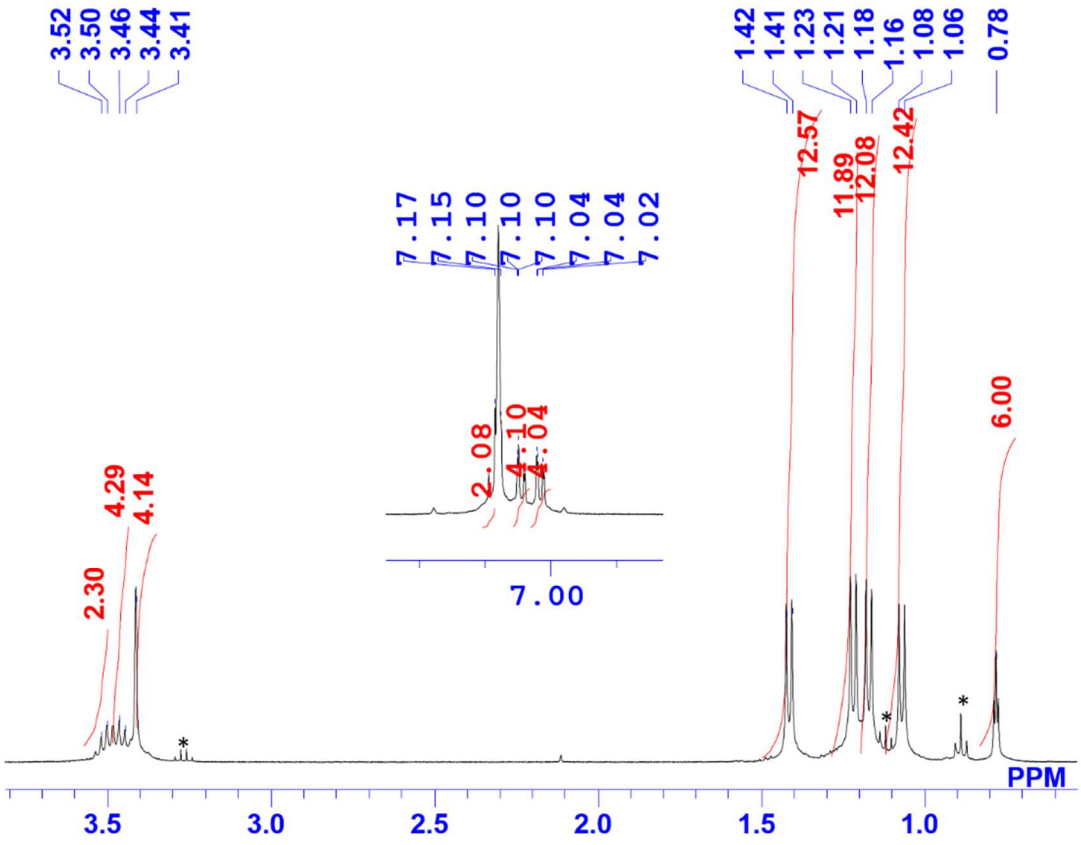

Figure S9. ^{1}H NMR spectrum of **124** (* denotes signal of *n*-hexane and Et_2O)

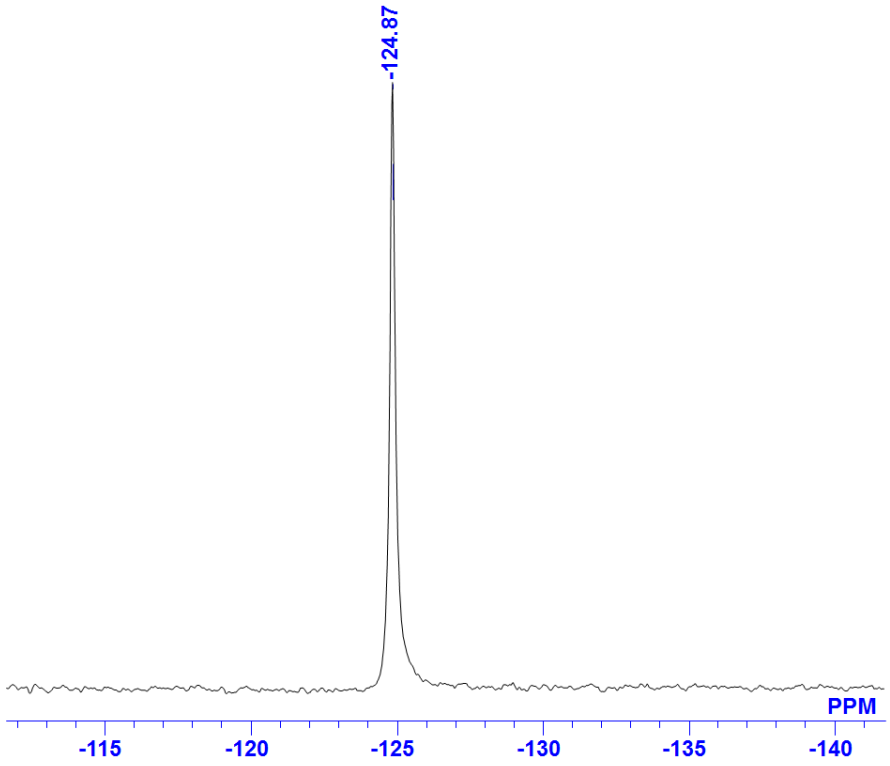

Figure S10. ^{31}P NMR spectrum of **124**

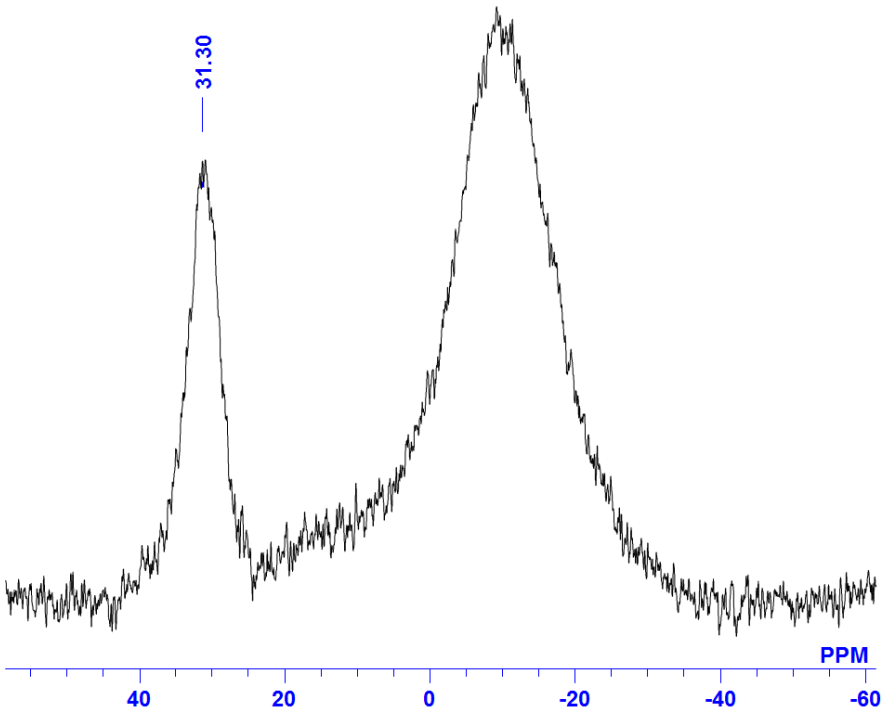

Figure S11. ^{11}B NMR spectrum of **124**

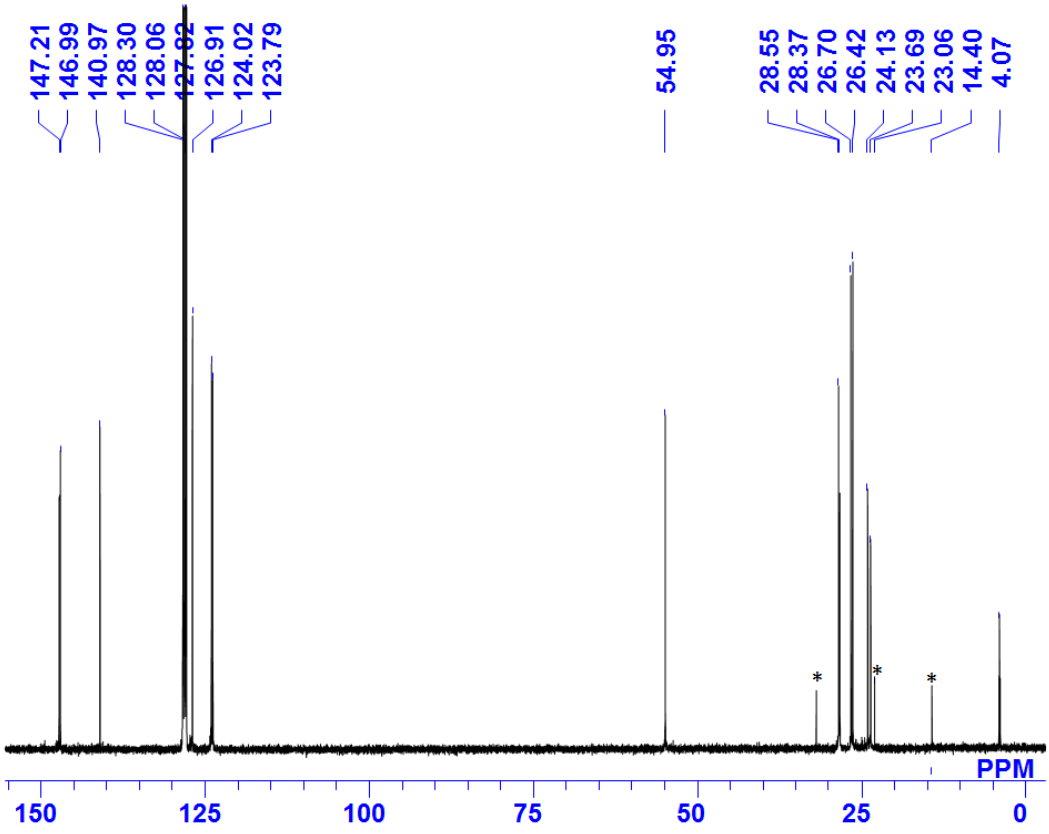

Figure S12. ^{13}C NMR spectrum of **124** (* denotes signal of *n*-hexane)

Estimation for the NMR yield of 124 from 113

In a glovebox, toluene (3.8 mL) was added to a mixture of **113** (30.0 mg, 35.7 μmol) and Li powder (24.7 mg, 3.57 mmol) in a 15 mL vial at room temperature. The color of the resulting solution rapidly turned into red. After the reaction mixture was stirred at room temperature for 1.5 h, the resulting suspension was filtered through a pad of Celite® to remove an excess amount of Li powder. The resulting mixture was added to a toluene solution (5 mL) of MeI (13.3 μL, 0.214 mmol) in a 30 mL vial. The resulting suspension was filtered through a pad of Celite® to remove insoluble salts. After removal of the volatiles from the filtrate, a solution of anthracene (12.7 mg, 71.4 μmol, 2 eq to **113**) in C_6H_6 (2 mL) was added to the reaction mixture as an internal standard. After removal of the volatiles, C_6D_6 (1 mL) was added to the residue. An aliquot (0.13 mL) of the resulting C_6D_6 solution was transferred to an NMR tube, and C_6D_6 (0.6 mL) was added to the tube. The NMR yield was estimated to be of 78% by comparison of the integral ratio of methyl protons in **124** with those of the protons at 9- and 10-positions in anthracene.

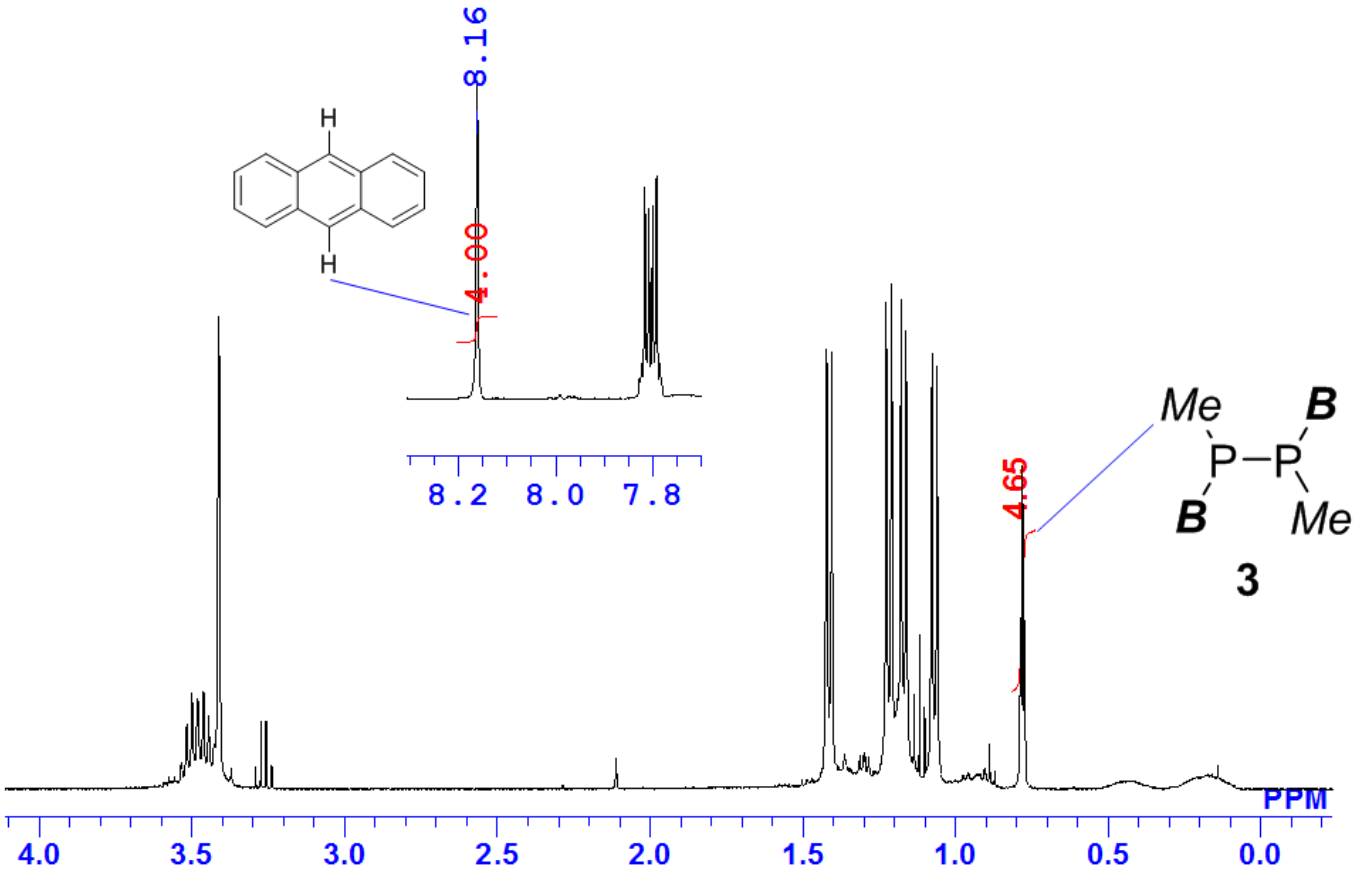

Figure S13. The ^{1}H NMR spectrum of the reaction mixture of **124**

2. Details for X-Ray Crystallography

Details of the crystal data and a summary of the intensity data collection parameters **123**, **123**·[DMAP]$_2$ and **124** are listed in Table S1.In each case a suitable crystal was mounted with a mineral oil to the glass fiber and transferred to the goniometer of a VariMax Saturn CCD diffractometer with graphite-monochromated Mo Kα radiation (λ = 0.71075 Å). All the following procedure for analysis, Yadokari-XG 2009 was used as a graphical interface.[10] The structures were solved by direct method with (SIR-2014 and SIR-97)[11] and refined by full-

matrix least-squares techniques against F^2 (SHELXL-2014).[12] The intensities were corrected for Lorentz and polarization effects or NUMABS program (Rigaku 2005). The non-hydrogen atoms were refined anisotropically. Hydrogen atoms were placed using AFIX instructions.

Table S1. Crystallographic data and structure refinement details for **123**, [**123**]·[DMAP]$_2$, and **124**

	[**123**]	[**123**]·[DMAP]$_2$	[**124**]
Empirical formula	$C_{52}H_{76}B_2Li_2N_4P_2$	$C_{80}H_{112}B_2Li_2N_8P_2$	$C_{54}H_{82}B_2N_4P_2$
Formula weight	854.6	1283.21	870.9
T (K)	93	93	93
λ (Å)	0.71075	0.71075	0.71075
Crystal system	Monoclinic	Triclinic	Orthorhombic
Space group	$P2_1/n$	P-1	Pbca
a (Å)	12.723(4)	12.039(2)	20.6963(15)
b (Å)	14.277(4)	12.447(3)	40.473(3)
c (Å)	14.695(4)	13.506(3)	25.1022(18)
α (°)	90	87.477(9)	90
β (°)	109.742(5)	87.628(9)	90
γ (°)	90	67.442(5)	90
V (Å^3)	6163(3)	1866.7(7)	21027(3)
Z	2	1	16
$D_{calc,}$ (g/m^3)	1.13	1.141	1.1
μ (mm^{-1})	0.124	0.106	0.121
F(000)	924	694	7584
Crystal size (mm)	0.26×0.16×0.08	0.16×0.15×0.15	0.30×0.18×0.07
2θ range (°)	3.197 to 25.999	2.998 to 27.468	3.020 to 28.000
reflns collected	18294	15458	162750
Indep reflns/ R_{int}	4860/0.0622	8234/0.0366	25310/0.0903
param	288	485	1153
GOF on F^2	1.15	0.999	1.071
R_1, wR_2 [I>2σ(I)]	0.0700, 0.1944	0.0560, 0.1217	0.0878, 0.2005
R_1, wR_2 (all data)	0.0913, 0.2349	0.0871, 0.1405	0.1225, 0.2297

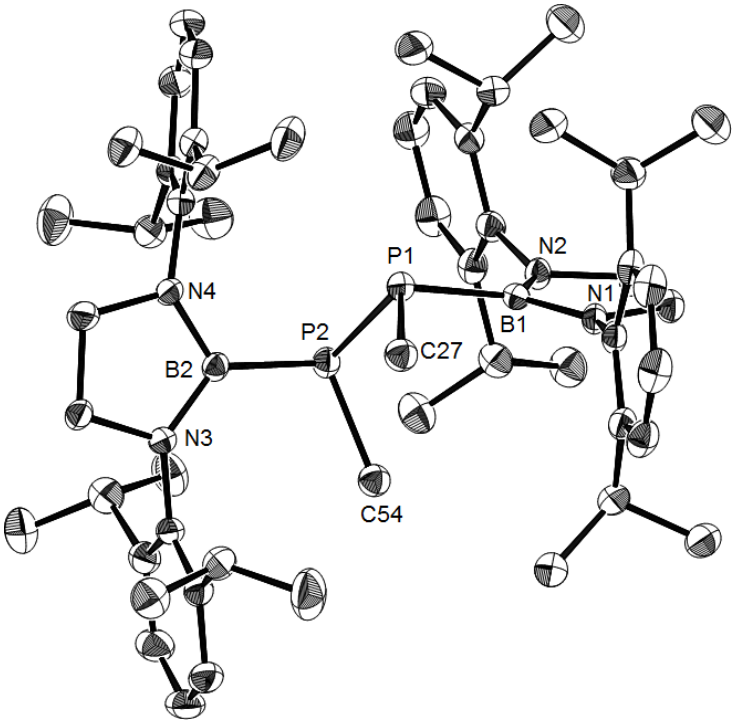

Figure S14. Molecular structure of **124** (thermal ellipsoids set at 50% probability, hydrogen atoms are omitted for clarity)

3. Computational Detail

The geometry optimizations were performed at the B3LYP[13]/6-31G(d)[14] level of theory by using Gaussian 09 program package[15] and each crystal structure as an initial geometry. The optimized structure was confirmed to have no imaginary frequency and could reproduce the X-ray structure (Figure S15 and S16 for MOs, Figure S17 for labels of atoms, XMol file for visualization is also available as Supporting Information).. At the optimized structures, natural bond orbital (NBO) analysis were performed at B3LYP[13]/6-31G(d)[14] level of theory for estimation of Wiberg bond index (WBI) and Mulliken atomic densities by using NBO 3.0 package embedded in Gaussian program.[15] (Tables S2 and S3). The TD-DFT calculation[16] was performed at the B3LYP[13]/6-31G(d)[14] level of theory (Table S4).

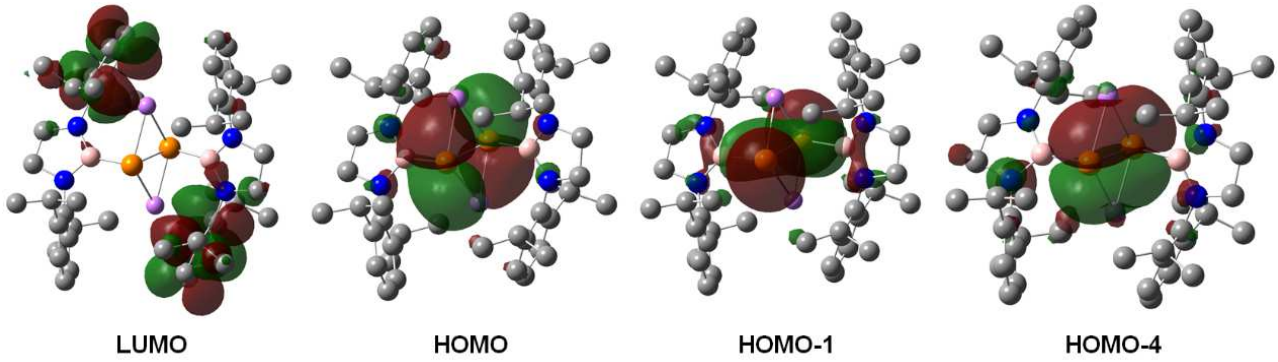

Figure S15. Selected molecular orbitals of **123** calculated at the B3LYP/6-31G(d) level of theory (hydrogen atoms omitted for clarity, gray: carbon, blue: nitrogen, orange: phosphorus, pale peach: boron, purple: lithium)

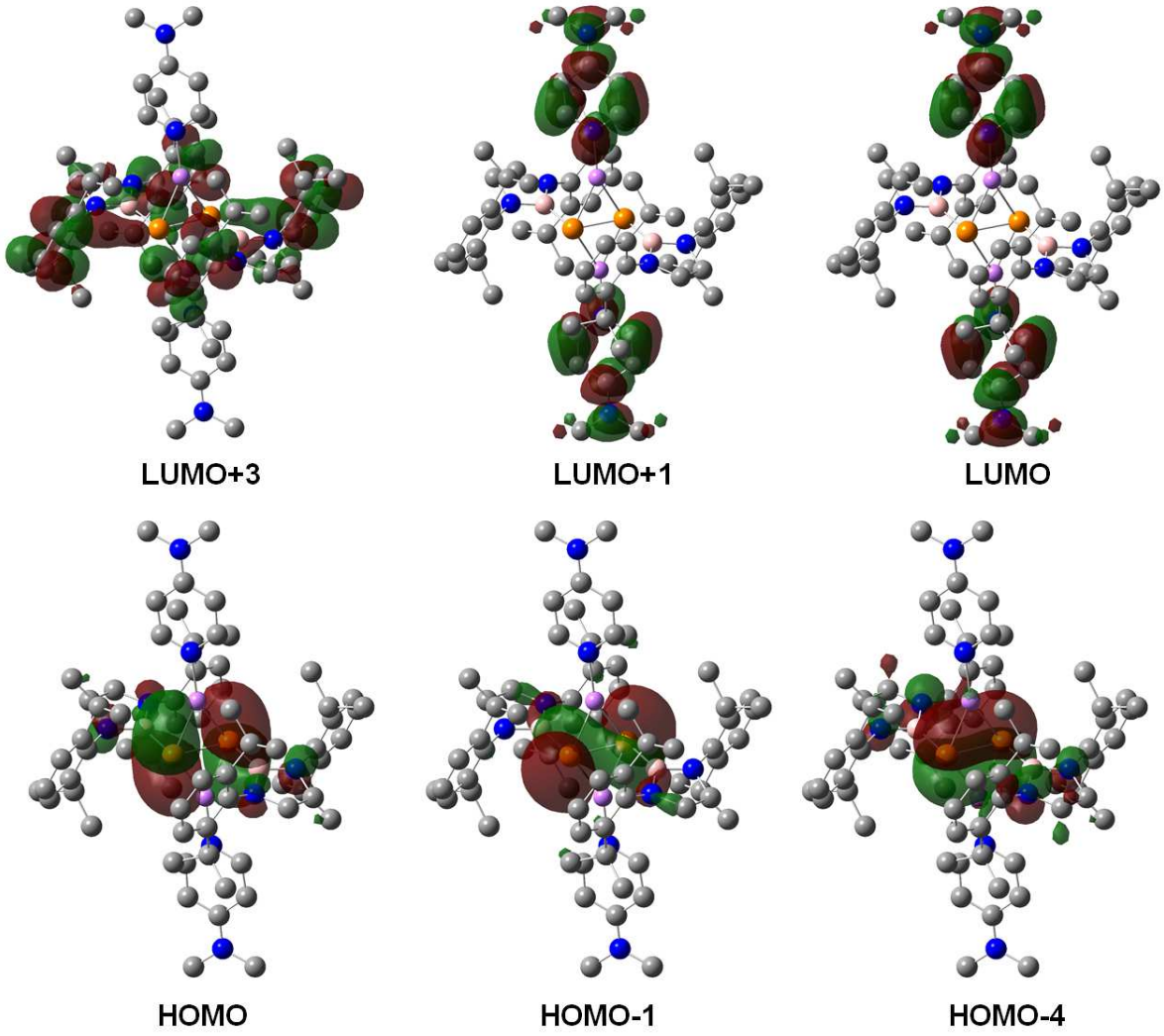

Figure S16. Selected molecular orbitals of **123**·$[DMAP]_2$ calculated at the B3LYP/6-31G(d) level of theory (hydrogen atoms are omitted for clarity, gray: carbon, blue: nitrogen, orange: phosphorus, pale peach: boron, purple: lithium)

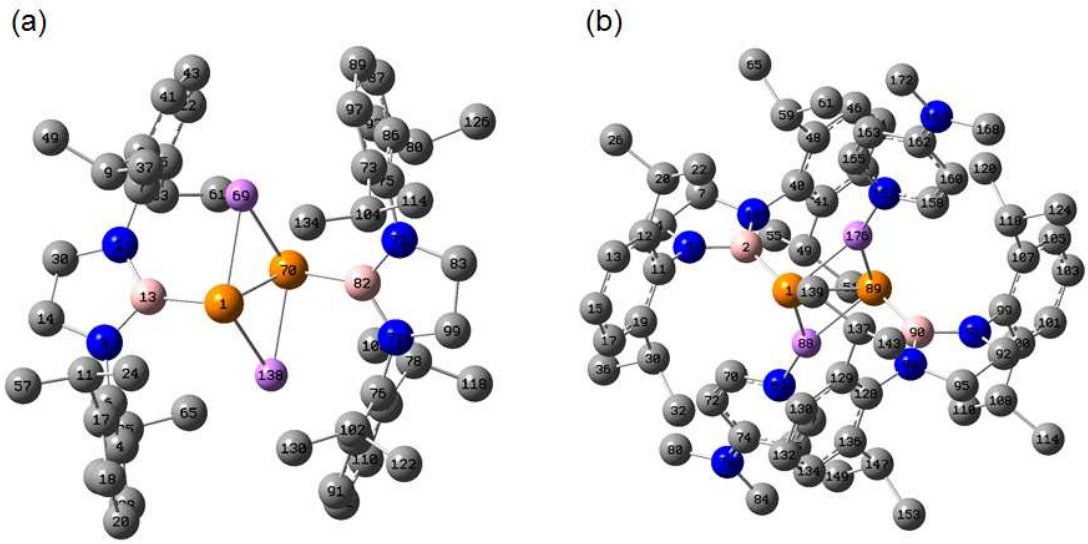

Figure S17. The optimized structures of (a) **123**, (b) **123**·[DMAP]$_2$

Table S2. Selected Mulliken charges, Wiberg bond indexes (WBI), donor-acceptor interaction (kcal/mol) in **2**

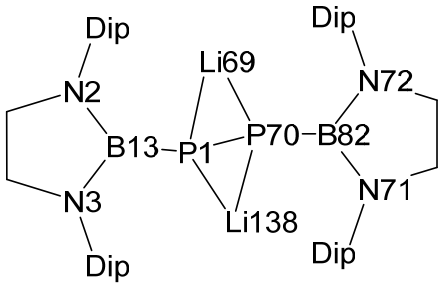

atom	charge	bond	WBI	donor	acceptor	interaction
P1	-0.208602	P1-P70	0.9413	P1	B13	20.50
P2	-0.213855	P1-B3	1.1766	P70	B82	0.82
B3	0.422916	P70-B82	1.1183	N2	B13	57.85
B70	0.444097	B13-N2	0.8816	N3	B3	60.38
N4	-0.542480	B13-N3	0.9159	N71	B82	60.11
N11	-0.549482	B82-N71	0.8990	N72	B82	62.60
N71	-0.543829	B82-N72	0.9234	P1-P70	B3	2.16
N78	-0.544001			P1-P70	B82	4.39

Table S3. Selected Mulliken charges, Wiberg bond indexes (WBI), donor-acceptor interaction (kcal/mol) in **123**·[DMAP]$_2$

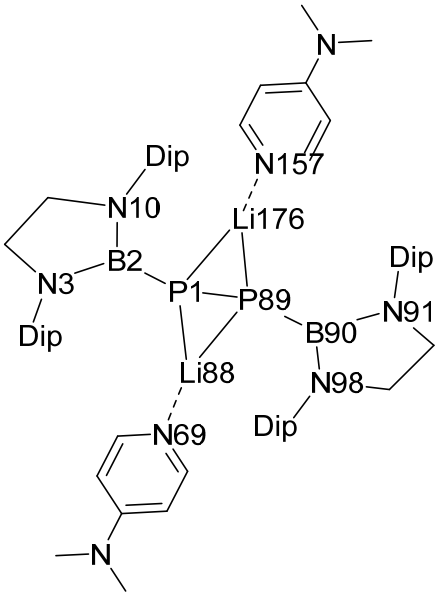

atom	charge	bond	WBI	donor	acceptor	interaction
P1	-0.187585	P1-P89	0.9868	P1	B2	49.56
P89	-0.187585	P1-B2	1.2693	P89	B90	49.56
B2	0.425144	P89-B90	1.2693	N3	B2	52.10
B90	0.425144	B2-N3	0.8798	N10	B2	55.42
N3	-0.560336	B2-N10	0.8897	N91	B90	55.42
N10	-0.567451	B90-N91	0.8798	N98	B90	55.42
N91	-0.560336	B90-N98	0.8897			
N98	-0.567451					

Table S4. Calculated excitation energies of **123**·[DMAP]$_2$ by TD-DFT method [CAM-B3LYP/6-31G(d)] (HOMO = 297)

Excited State 1: Singlet-AG 3.1999 eV 387.47 nm f=0.0000 <S**2>=0.000
297 -> 298 0.69412
Excited State 2: Singlet-AU 3.2284 eV 384.04 nm f=0.0143 <S**2>=0.000
297 -> 299 0.70306
Excited State 3: Singlet-AU 3.4438 eV 360.02 nm f=0.0014 <S**2>=0.000
297 -> 300 0.70571
Excited State 4: Singlet-AG 3.4460 eV 359.79 nm f=0.0000 <S**2>=0.000
297 -> 301 0.70574
Excited State 5: Singlet-AU 3.7798 eV 328.02 nm f=0.0132 <S**2>=0.000
297 -> 302 0.48734
297 -> 311 0.15508
297 -> 314 -0.41006

297 -> 316 -0.11502

297 -> 320 0.15201

Excited State 6: Singlet-AG 3.9668 eV 312.55 nm f=0.0000 <S**2>=0.000

297 -> 298 -0.11517

297 -> 303 0.56390

297 -> 310 -0.12149

297 -> 312 0.33176

297 -> 317 0.12301

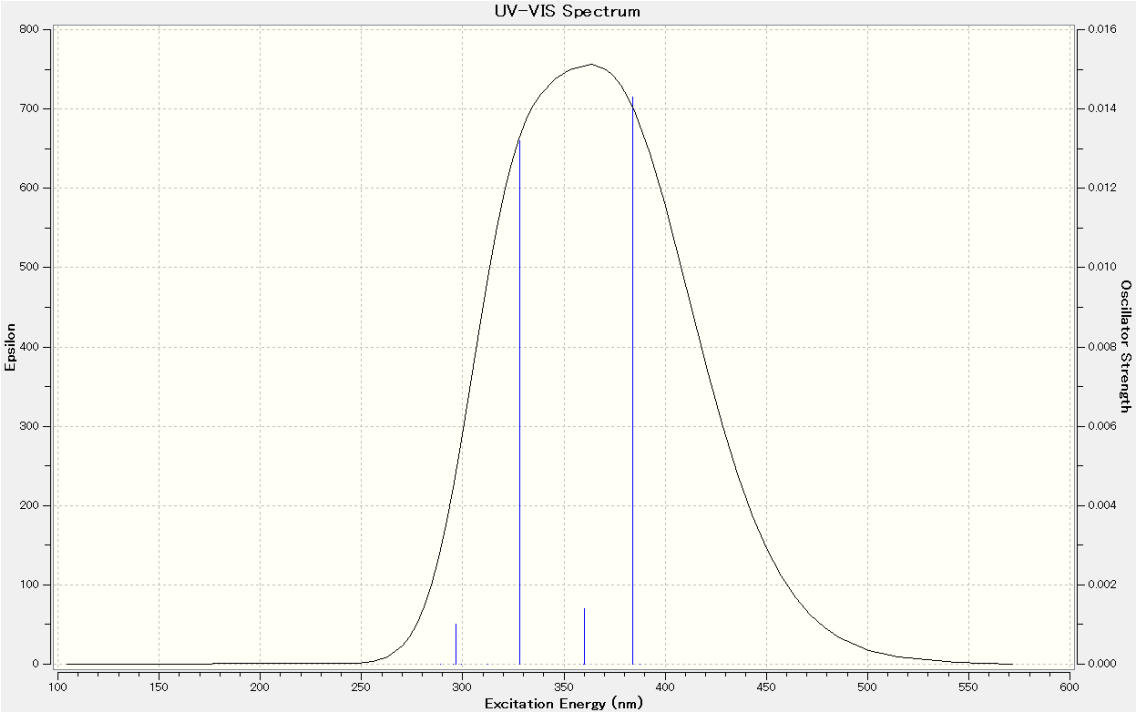

Figure S18. Simulated UV-vis spectrum of **123**·$[DMAP]_2$ by TD-DFT calculations.

Reference

1. Pestana, D. C.; Power, P. P. *J. Am. Chem. Soc.* **1989**, 111, 6887.

2. (a) Yoshifuji, M.; Shima, I.; Inamoto, N.; Hirotsu, K.; Higuchi, T. *J. Am. Chem. Soc.* **1981**, *103*, 4587. (b) Yoshifuji, M.; Shima, I.; Inamoto, N.; Hirotsu, K.; Higuchi, T. *J. Am. Chem. Soc.* **1982**, *104*, 6167.

3. (a).Cetinkaya, B.; Hudson, A.; Lappert, M. F.; Goldwhite, H. *J. Chem. Soc., Chem. Commun.* **1982**, 609. (b) Culcasi, M.; Gronchi, G.; Escudié, J.; Couret, C.; Pujol, L.; Tordo, P. *J. Am. Chem. Soc.* **1986**, *108*, 3130. (c) Bard, A. J.; Cowley, A. H.; Kilduff, J. E.; Leland, J. K.; Norman, N. C.; Pakulski, M.; Heath, G. A. *J. Chem. Soc. Dalton Trans.* **1987**, 249. (d) Shah, S.; Burdette, S. C.; Swavey, S.; Urbach, F. L.; Protasiewicz, J. D. *Organometallics* **1997**, *16*, 3395. (e) Dutan, C.; Shah, S.; Smith, R.C.; Choua, S.; Berclaz, T.; Geoffroy, M.; Protasiewicz, J. D. *Inorg. Chem.* **2003**, *42*, 6241. (f) Sasamori, T.; Mieda, E.; Nagahora, N.; Sato, K.; Shiomi, D.; Takui, T.; Hosoi, Y.; Furukawa, Y.; Takagi, N.; Nagase, S.; Tokitoh, N. *J. Am. Chem. Soc.* **2006**, *128*, 12582. (g) Nagahora, N.; Sasamori, T.; Hosoi, Y.; Furukawa, Y.; Tokitoh, N. *J. Organomet. Chem.* **2008**, *693*, 625.

4. (a) Bartlett, R. A.; Feng, X.; Power, P. P. *J. Am. Chem. Soc.* **1986**, *108*, 6817. (b) Bartlett, R. A.; Dias, H. V. R.;

Feng, X.; Power, P. P. *J. Am. Chem. Soc.* **1989**, *111*, 1306. (c) Pestana, D. C.; Power, P. P. *J. Am. Chem. Soc.* **1991**, *113*, 8426.

5. (a) Asami, S.-s.; Okamoto, M.; Suzuki, K.; Yamashita, M. *Angew. Chem. Int. Ed.* **2016**, *55*, 12827. (b) Asami, S.-s.; Ishida, S.; Iwamoto, T.; Suzuki, K.; Yamashita, M. *Angew. Chem. Int. Ed.* **2017**, *56*, 1658.

6. (a) Issleib, K.; Krech, K. *Chem. Ber.* **1966**, *99*, 1310. (b) Baudler, M.; Grüner, C.; Fürstenberg, G.; Kloth, B.; Saykowski, F.; Özer, U. Z. *Anorg. Allg. Chem.* **1978**, *446*, 169. (c) Baudler, M.; Tschäbunin, H.; Suchomel, H.; Hasenbach, J. *Z. Naturforsch. B* **1994**, *49*, 773. (d) Geier, J.; Rüegger, H.; Wörle, M.; Grützmacher, H. *Angew. Chem. Int. Ed.* **2003**, *42*, 3951. (e) Stein, D.; Dransfeld, A.; Flock, M.; Rüegger, H.; Grützmacher, H. *Eur. J. Inorg. Chem.* **2006**, 4157.

7. The Elements, 3rd ed.; Oxford University Press: New York. 1998.

8. IUPAC recommends to use "boranuida" as a replacement name of an anionic boron atom for organic molecules. see, Favre, H. A. Powell, W. H., *Nomenclature of Organic Chemistry : IUPAC Recommendations and Preferred Names 2013*. The Royal Society of Chemistry.

9. Märkl, G.; Sejpka, H. *Tetrahedron Lett*. **1986**, *27*, 171.

10. (a) Wakamiya, A.; Mori, K.; Araki, T.; Yamaguchi, S. *J. Am. Chem. Soc.* **2009**, *131*. 10850. (b) Araki, T.; Wakamiya, A.; Mori, K.; Yamaguchi, S. *Chem. Asian J.* . **2012**, *7*, 1594.

11. Kabuto, C.; Akine, S.; Kwon, E., *J. Cryst. Soc. Jpn.* **2009**, *51*, 218.

12. Altomare, A.; Burla, M. C.; Camalli, M.; Cascarano, G. L.; Giacovazzo, C.; Guagliardi, A.; Moliterni, A. G. G.; Polidori, G.; Spagna, R. *J. Appl. Crystallogr.* **1999**, *32*, 115. (b) Burla, M. C.; Caliandro, R.; Carrozzini, B.; Cascarano, G. L.; Cuocci, C.; Giacovazzo, C.; Mallamo, M.; Mazzone, A. Polidori, G. *J. Appl. Crystallogr.* **2015**, *48*, 306.

13. (a) Sheldrick, G. *Act. Cryst. Sec. A* **2008**, *64*, 112. (b) Sheldrick, G. *Act. Cryst. Sec. C* **2015**, *71*, 3.

14. (a) Lee, C.; Yang, W.; Parr, R. G. *Phys. Rev. B* **1988**, *37*, 785. (b) Becke, A. D. *Phys. Rev. A* **1988**, *38*, 3098; (c) Miehlich, B.; Savin, A.; Stoll, H.; Preuss, H. *Chem. Phys. Lett.* **1989**, *157*, 200. (d) Becke, A. D. *J. Chem. Phys.* **1993**, *98*, 5648. (e) Stephens, P. J.; Devlin, F. J.; Chabalowski, C. F.; Frisch, M. J. *J. Phys. Chem.* **1994**, *98*, 11623.

15. Huzinaga, S.; Andzelm, J.; Klobukowski, M.; Radzio-Andzelm, E., Sakai, Y.; Tatewaki, H., *Gaussian basis sets for molecular calculations.* Elsevier: **1984**.

16. Reed, A. E.; Curtiss, L. A.; Weinhold, F. *Chem. Rev.* **1988**, *88*, 899.

17 (a) Casida, M. E.; Jamorski, C.; Casida, K. C.; Salahub, D. R. *J. Chem. Phys.* **1998**, *108*, 4439. (b) Stratmann, R.; E.; Scuseria, G. E.; Frisch, M. J. *J. Chem. Phys.* **1998**, *109*, 8218. (c) Van Caillie, C.; Amos, R. D. *Chem. Phys. Lett.* **1999**, 308, 249. (d) Van Caillie, C.; Amos, R. D. *Chem. Phys. Lett.* **2000**, *317*, 159. (e) Scalmani, G.; Frisch, M. J.; Mennucci, B.; Tomasi, J.; Cammi, R.; Barone, V. *J. Chem. Phys.* **2006**, *124*, 94107.

Chapter 5

Conclusion and Perspectives

5.1 Conclusion

Throughout this thesis, the author systematically studied the effecets of the boryl-substituents on the properties of P=P double bond and related species. The following is the short summary for each chapters.

In chapter 2, the author reported the first synthesis of the boryl-substituted diphosphene, which has almost orthogonal relationship between the two boron containing planes and the plane of B-P=P-B moiety double bond. DFT calculations revealed that the boryl-substituent works as stronger σ-donor than that of the phenyl substituent (Figure 1), although σ-donating effect of the boryl-substitutent is slightly weaker than Mes* substituent. In addition, the π-acceptor property of boryl-substituent was found to play an important role in the thermodynamic stability of phosphinophosphide, generated as ^{n}BuLi adduct of the diboryldiphosphene, due to pπ–pπ interaction between B and P.

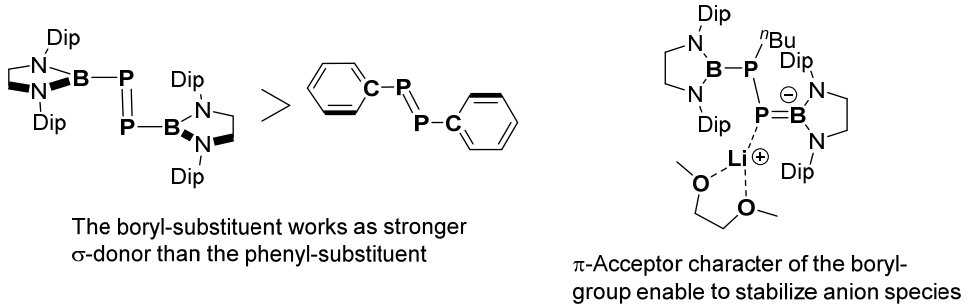

Figure 1. Effects of the boryl-substituent in the diboryldiphosphene and boryl-substituted phosphinophosphide

In chapter 3, the author described the isolation of the diboryldiphosphene radical anion as the first example of the structuraly characterized of diphosphene radical anion. X-ray structures of the radical anions showed a weakened the P=P double bond and a relatively weak pπ–pπ interaction between B and P. Moreover, ESR spectroscopy and DFT calculations showed that the unpaired electron is delocalized over the B-P=P-B moiety (Figure 2).

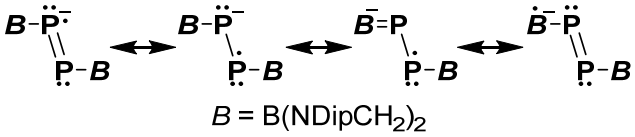

Figure 2. Resonance structures of diboryldiphosphene radical anion

In chapter 4, the author revealed the structure and reactivity of the boryl-substituted diphosphanediide, which was generated by reduction of the boryl-substituted diphosphene with an excess amount of Li (Figure 3). In addition, X-ray structure and DFT calculations of the boryl-substituted diphosphenediide-DMAP complex showed a 1,4-diboranuida-2,3-diphosphabuadiene (B^{-}=P-P=B^{-}) character. This compound has a characteristic absorption at λ_{max} = 380 nm, which could be assigned as an intramolecular charge transfer from π-orbital of B=P-P=B moiety to π*-orbital of DMAP ligand by TD-DFT calculations (Figure 3).

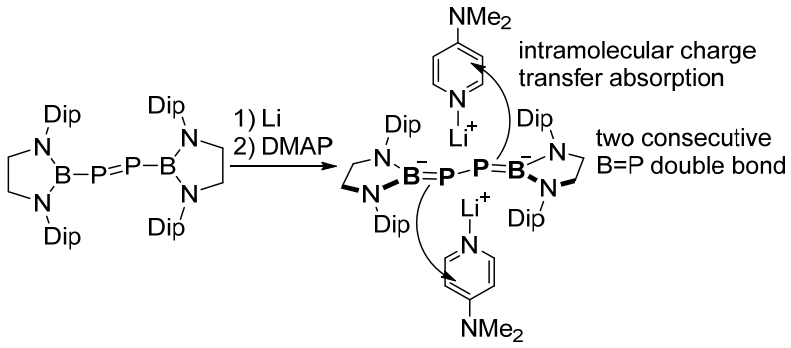

Figure 3. Properties of boryl-substituted diphosphanediide DMAP complex

5.2 Perspective

Although this thesis revealed the importance of π-acceptor property of the boryl-substituent, the introduction of boryl group is limited to that of diamino group at present. Diaminoboryl group has a lower Lewis acidity than that of dialkylboryl group, because of the existence of electron donation of nitrogen to boron. Actually, In the boryl-substituted diphosphene radical anion, mainly spin density is delocalized on two phosphorus. Thus, the author feels the importance of Lewis acidity of boryllithium. Meanwhile, Lewis acidity of NHC [N-heterocyclic carbene], which has isoelectronic structure of boryllithium, can be tuned by its molecular design. For example, CAAC [Cyclic(alkyl)(amino)carbene],[1] in which one nitrogen atom of NHC is replaced with carbon atom, has much stronger Lewis acidity and σ-donor property in comparison with NHC. Because carbon atom has smaller electronegativity than that of nitrogen atom. In addition, one of electron donating nitrogens was decreased. Recently, Kinjo has also reported cyclic(alkyl)(amino)germylene, which has lower LUMO energy than diaminogermylene.[2] Thus, the author believes (alkyl)(amino)boryllithium has stronger Lewis acidity and σ-donor property than diaminoboryllithium. Moreover, (alkyl)(amino)boryl-substituted diphosphene would express narrower HOMO-LUMO gap than diaminoboryl-substituted diphosphene.

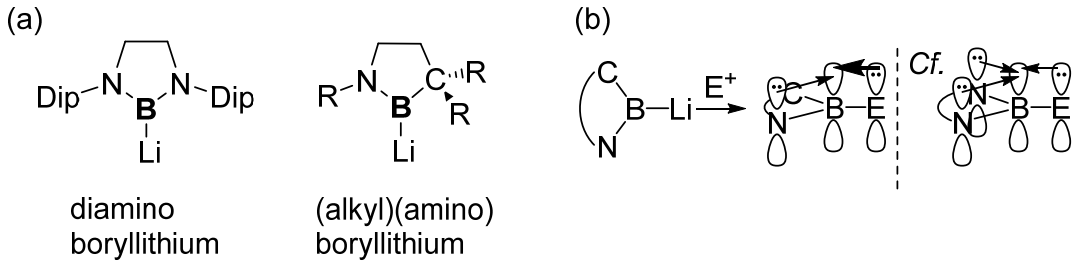

Figure 4. (a) Structural comparison between diaminoboryllithium and cyclic(alkyl)(amino)boryllithium (b) Reaction of (amino)(alkyl)boryllithium with E^+ and pπ-pπ interaction in products

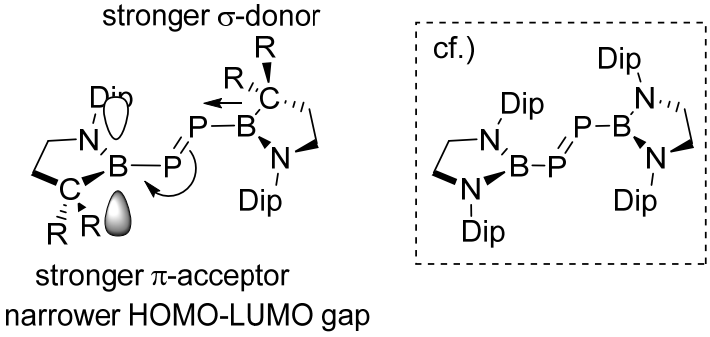

Figure 5. Property of (alkyl)(amino)boryl-substituted diphosphene

Reference

(1) Lavallo, V.; Canac, Y.; Prasang, C.; Donnadieu, B.; Bertrand, G. *Angew Chem Int ed.* **2005,** *44*, 5705.

(2) Wang, L.; Lim, Y. S.; Li, Y.; Ganguly, R.; Kinjo, R. *Molecules*, **2016,** *21*, 990.

Publication List

(1) Asami, S.-s.; Okamoto, M.; Suzuki, K.; Yamashita, M.

"A Boryl-Substituted Diphosphene: Synthesis, Structure, and Reactivity with ^{n}BuLi to Form An Isolable Adduct Stabilized by pπ-pπ Interactions"

Angew. Chem. Int. Ed. **2016,** *55,* 12827-12831.

DOI: 10.1002/anie.201607995

(2) Asami, S.-s.; Ishida, S.; Iwamoto, T.; Suzuki, K.; Yamashita, M.

"Isolation and Characterization of Radical Anions Derived from a Boryl-Substituted Diphosphene"

Angew. Chem. Int. Ed. **2017,** *56,* 1658-1662.

DOI: 10.1002/anie.201611762

(3) Asami, S.-s.; Suzuki, K.; Yamashita, M.

"Two-Electron Reduction of Diboryldiphosphene: Formation of Intramolecular Charge Transfer Complex of Dianionic B=P–P=B Species"

C*hem. Lett.* 2017, accepted

Reference

(1) Yamaoka, M.; Asami, S.-s.; Funaki, N.; Kimura, S.; Yingjie, L.; Fukuda, T.; Yamashita, M.

"**Preparation of Organic Light-Emitting Diode Using Coal Tar Pitch, a Low-Cost Material, for Printable Devices**"

PLOS ONE. **2013,** *8,* e62903.

DOI:10.1371/journal.pone.0062903

Acknowledgement

The author would express his deep gratitude to Professor Makoto Yamashita for his continuous guidance, useful discussion, developing a favorable research environments, and hearty encouragement during the course of this work. Dr. Katsunori Suzuki and Dr. Kwan Huang, Enrique. are deeply acknowledged for helpful discussion, experimental guidance, hearty advice, and encouragement throughout the course of the studies.

The author is appreciative to the members of his thesis committee, Professor Youichi Ishii, Professor Tamejiro Hiyama, Professor Shin-ichi Fukuzawa, Professor Hirohiko Sato, and Professor Takayuki Kawashima, for their instructive and helpful discussions.

The author is sincerely indebted to Mr. Masafumi Okamoto, who has contributed to the work described in Chapter 2.

The author appreciates Professor Takeaki Iwamoto and Associate Professor Shintaro Ishida for ESR measurement in Chapter 3.

The author appreciates sincerely grateful to the members of Yamashita laboratory, Mr. Hayato Ogawa, Mr. Sei Kamakura, Mr. Kosuke Shimada, Mr. Takuma Miyata, Mr. Hiroki Asakawa, Mr. Kaoru Onuma, Mr. Yasushi Kawai, Mr. Shinya Nema, Mr. Sho Fujimoto, Mr. Nakamura Taichi, Mr. Takuya Ishii, Mr. Takuto Ohsato, Mr. Haruki Kisu, Ms. Chiemi Kojima, Ms. Mao Noguchi, Mr. Shuji Asanuma, Mr. Ryo Kitamura, Ms. Nana Tsukahara, Ms. Rona Yamazaki, Mr. Seiya Watanabe, Mr. Seiji Akiyama,.Mr. Jun Kondo, Mr. Yuhei Katsuma, Mr. Shin Nakayama, Mr. Jun Kobayashi, Mr. Shuhei Takamori, Mr. Kohei Hayashi, Mr. Yutaro Ishikawa, Mr. Kanon Kaiya, Mr. Reiji Kurumada and Mr. Atumi Yagi. The author would like to thank Ms. Tomoko Yoshida for kind assistance

Finally, the author would like to express his sincere acknowledgment to his family, Mr. Yuichi Asami, Ms. Yumi Asami, Mr. Takao Asami, and Ms. Sizue Asami for their continuous encouragement and their financial support.